JEM Journal of Experimental Medicine

ARTICLE

RORγt eTACs mediate oral tolerance and Treg induction

Im-Hong Sun[1,2*], Anita E. Qualls[2*], Han S. Yin[2*], Jiaxi Wang[2*], Matthew P. Arvedson[2], Joe Germino[2], Nolan K. Horner[1,2], Sheng Zhong[1,2], Juan Du[1,2], Martin Valdearcos[2], Vasilis Ntranos[2,3], Richard M. Locksley[4,5,6], Roberto R. Ricardo-Gonzalez[7], and James M. Gardner[1,2]

The immune system must distinguish pathogens from innocuous dietary antigens, but the precise mechanisms and cellular actors remain unclear. Here, we demonstrate that RORγt-lineage APCs are required for oral tolerance. Using lineage tracing and single-cell sequencing, we show these APCs consist of three principal populations: type 3 innate lymphoid cells (ILC3s), RORγt-lineage dendritic cells, and cells expressing Aire called RORγt eTACs (R-eTACs)—also known as Janus or Thetis cells. We show that R-eTACs, but not ILC3s, are required for oral tolerance induction. We find R-eTACs are of probable myeloid origin and uniquely express integrin β8 (Itgb8). Both MHCII and Itgb8 expression in RORγt-lineage cells are necessary to induce food-specific regulatory T cells. Mice lacking R-eTACs or with deletion of MHCII or Itgb8 in the RORγt lineage fail to generate Tregs and instead develop a T-follicular helper response with elevated antigen-specific antibodies. These findings establish R-eTACs as critical mediators of oral tolerance and suggest novel cellular targets to modulate immune tolerance.

Introduction

Food allergies are increasingly prevalent worldwide, but effective treatments and prevention strategies are lacking (Dunlop and Keet, 2018; Garkaby et al., 2021; Vale et al., 2021). While it is known that food allergy arises from inappropriate immune reactivity to orally digested dietary antigens, there is limited understanding of oral tolerance mechanisms and the APC populations involved. Conventional dendritic cells (cDCs) have been suggested as key players in tolerance against both commensal and dietary antigens via induction of antigen-specific regulatory T cells (Tregs) in the mesenteric lymph nodes (mLN) (Coombes et al., 2007; Esterházy et al., 2016, 2019; Loschko et al., 2016; Mazzini et al., 2014; Pabst and Mowat, 2012; Worbs et al., 2006). However, recent reports suggest that RORγt$^+$ APCs, not cDCs, induce tolerance to intestinal commensal bacteria and are specifically required for the peripheral induction of RORγt$^+$ Tregs (Akagbosu et al., 2022; Kedmi et al., 2022; Lyu et al., 2022a). We thus sought to determine whether and which RORγt-lineage APCs are also involved in the induction of oral tolerance and better define their identity, lineage, and taxonomy.

We and others have recently described unique APC populations that express varied levels of Aire and RORγt and high levels of major histocompatibility complex class II (MHCII) referred to by several names including Janus cells (JCs) (Wang et al., 2021), Thetis cells (TCs) (Akagbosu et al., 2022), Aire$^+$ ILC3 or ILC3-like cells (Yamano et al., 2019; Dobeš et al., 2022), and RORγt$^+$ eTACs (Abramson et al., 2023). We have previously shown eTACs to be capable of inducing cognate CD4 and CD8 T cell tolerance (Gardner et al., 2008, 2013; Wang et al., 2021). Recently, the term "RORγt$^+$ eTACs" was suggested as a consensus nomenclature for this population (Abramson et al., 2023) and will be utilized here, with the understanding that this remains an actively evolving field. We show that RORγt-lineage APCs induce oral antigen-specific Treg differentiation while suppressing T follicular helper cell (Tfh) development. We utilize lineage tracing and single-cell sequencing to show that RORγt eTACs (R-eTACs), innate lymphoid cells (ILCs)/lymphoid tissue inducer cells (LTis), and subsets of dendritic cells (DCs) are the three principal RORγt-lineage APC populations in mouse secondary lymphoid organs (SLOs), and are consistent across both age and location. While ILCs and LTis are of lymphoid lineage, mixed bone marrow chimera (BMC) studies using genetic knockout models reveal that R-eTACs are of myeloid lineage. Further, while mice lacking MHCII in all RORγt-lineage

[1]Department of Surgery, University of California, San Francisco, San Francisco, CA, USA; [2]Diabetes Center, University of California, San Francisco, San Francisco, CA, USA; [3]Department of Epidemiology and Biostatistics, Computational Health Sciences Institute, University of California, San Francisco, San Francisco, CA, USA; [4]Department of Medicine, University of California, San Francisco, San Francisco, CA, USA; [5]Department of Microbiology and Immunology, University of California, San Francisco, San Francisco, CA, USA; [6]University of California, Howard Hughes Medical Institute, San Francisco, San Francisco, CA, USA; [7]Department of Dermatology, University of California, San Francisco, San Francisco, CA, USA.

*I.-H. Sun, A.E. Qualls, H.S. Yin, and J. Wang contributed equally to this paper. Correspondence to James M. Gardner: james.gardner@ucsf.edu.

APCs have impaired dietary antigen-specific Tregs and develop an exaggerated antibody response to food antigens, this can be fully rescued by bone marrow (BM) with functional R-eTACs but lacking ILCs/LTis. In contrast, in mice with selectively depleted R-eTACs, defects in oral tolerance persist. This process is independent of the Aire gene itself, but depends on integrin β8, which is highly enriched on R-eTACs. These findings highlight the critical role of R-eTACs in maintaining immune tolerance to dietary antigen, with potential implications for allergy and inflammation.

Results

RORγt-lineage APCs mediate oral tolerance to food antigen

Recent reports have demonstrated the essential role of antigen presentation by RORγt-lineage APCs in the induction of Tregs against commensal bacteria in the gut using *RORγt*^{Cre}×MHCII$^{fl/fl}$ (MHCII$^{\Delta RORγt}$) mice (Akagbosu et al., 2022; Hepworth et al., 2013, 2015; Kedmi et al., 2022; Lyu et al., 2022a). Like commensal tolerance, the immune system must also recognize and tolerate food antigens to prevent allergy, and thus, we sought to understand whether RORγt-lineage APCs are also crucial for inducing oral tolerance to dietary antigens. To monitor T cell responses against food, we adoptively transferred naïve OT-II CD4$^+$ T cells—specific for model dietary antigen chicken ovalbumin (OVA)—into wild-type (WT) or MHCII$^{\Delta RORγt}$ mice (Fig. 1 A). After 2 days of OVA feeding via oral gavage, we harvested the mLN, a site critical for T cell priming in the induction of tolerance to food antigens (Worbs et al., 2006). Compared to WT controls, MHCII$^{\Delta RORγt}$ mice had diminished RORγt$^+$ and RORγt$^-$ Tregs in OT-IIs (Fig. 1, B and C, gating strategy, Fig. S1 A). The induction of anergic T cell clones has also been implicated in oral tolerance (Chen et al., 1995; Friedman and Weiner, 1994; Hong et al., 2022), and indeed, MHCII$^{\Delta RORγt}$ mice exhibited decreased percentages of FR4$^+$CD73$^+$ anergic OT-IIs (Fig. S1 B). Consistent with previous reports, MHCII$^{\Delta RORγt}$ mice had decreased endogenous RORγt$^+$ Tregs and increased endogenous T helper 17 (Th17) cells, while endogenous RORγt$^-$ Tregs were not different from WT controls (Fig. S1 C). After 7 days of OVA feeding, MHCII$^{\Delta RORγt}$ mice had a similarly reduced percentage of OT-II Tregs and, interestingly, elevated Tfh cells in both the mLN and Peyer's patches (PP) (Fig. 1, D and E, gating strategy, Fig. S1 D).

MHCII$^{\Delta RORγt}$ mice develop gut dysbiosis in adulthood due to the absence of functional APC populations in early life (Akagbosu et al., 2022; Hepworth et al., 2013, 2015), which could impair oral tolerance simply as a secondary effect of generalized gut inflammation. To account for this, we generated BMCs with either WT or MHCII$^{\Delta RORγt}$ BM, such that these mice would have a normal gut immune environment during the early-life window. Indeed, after 8 wk of reconstitution followed by 7 days of OVA feeding, MHCII$^{\Delta RORγt}$ BMC mice had equivalent colon lengths to WT BMC mice (Fig. S1 E, top), no rectal prolapse (data not shown), and normal proportions of endogenous Th17 cells (Fig. S1 E, bottom). However, these mice retained profound defects in oral tolerance to dietary antigen, as OT-II RORγt$^+$ and RORγt$^-$ Tregs were significantly abolished in the mLN, PP, and small intestine lamina propria (siLP) (Fig. S1 F). Anergic OT-II T cells were also diminished across these organs, and OT-II Tfh cells were elevated in the mLN and PP (Fig. S1, F and G). Interestingly, OVA-specific Gata3$^+$ Tregs were also diminished in the siLP of MHCII$^{\Delta RORγt}$ mice (Fig. S1 H). These findings demonstrate that RORγt-lineage APCs are crucial for establishing tolerance against oral antigens via the induction of dietary antigen-specific Tregs.

Reconciling the diversity of RORγt-lineage APC populations

Previous attempts to define RORγt-lineage APC populations have used a range of genetic tools—largely transcriptional reporters for *Rorc* and *Aire*—but none have directly traced all RORγt-lineage APCs to establish consensus identities for the populations potentially responsible for the observed conditional knockout phenotypes. Thus, we performed next-generation gel bead-in emulsion (GEM-X) single-cell RNA sequencing (scRNA-seq) analysis on all RORγt-lineage APCs in mouse SLOs. We procured mLN, spleen, and other lymph nodes (LNs; cervical, inguinal, axillary, brachial, and para-aortic) from adult RORγt-lineage mice (*RORγt*^{Cre}×Rosa26-LSL-tdTomato) and FACS-sorted tdTomato$^+$ MHCII$^+$ cells for subsequent scRNA-seq.

We found that RORγt-lineage APCs consist of three main populations: ILCs/LTis, R-eTACs (previously referred to as JCs, TCs, and ILC3/ILC3-like Aire$^+$ cells), and RORγt-lineage DCs (R-DCs) (Fig. 2 A; and Fig. S2, A and B). All populations were enriched for tdTomato (tdTmt) reporter transcript, while only R-eTACs have appreciable levels of Aire-GFP reporter and Aire gene transcript (Fig. S2 C). R-eTACs were distributed across all SLOs and not unique to the mLN, contrary to previous reports (Akagbosu et al., 2022) (Fig. S2, D and E). R-DC subsets consist of *Xcr1*$^+$ *Itgax*^{hi} R-cDC1s, *Sirpa*$^+$ *Itgax*^{hi} R-cDC2s, and *Ccr7*$^+$ *Itgax*^{lo} R-migratory DCs (R-mDC).

R-eTACs were defined as transcriptionally distinct clusters expressing varied levels of *Aire* and *Rorc*, as previously described (Kedmi et al., 2022; Wang et al., 2021). *Aire* expression is highest in R-eTAC1s and R-eTAC3s, while *Rorc* expression is highest in R-eTAC2s. Using this high-resolution approach, additional subpopulations of proliferating R-eTACs (*Mki67*$^+$) and LTi-like-R-eTACs (*Cd4*$^+$ *Cxcr6*$^+$) were identified, which also expressed *Aire* and *Rorc* (Fig. 2, B and C). The expression of *Itgav* and *Itgb8* has been shown to be critical for RORγt$^+$ APCs to induce commensal-specific Tregs (Akagbosu et al., 2022; Kedmi et al., 2022), and here, we found *Itgav* and *Itgb8* expression highly enriched in R-eTACs, as well as in R-mDCs. All RORγt-lineage APCs also express some levels of *Icosl*, with R-eTAC subsets expressing the highest levels, which has potential relevance for Tfh interactions (Fig. S2 F). In addition, recent publications have highlighted several key markers including *Prdm16*, *Thrb*, *Il4i1*, and *Ube2e2* that identified tolerogenic, RORγt-expressing APCs in both humans and mice (Ulezko Antonova et al., 2023; Fu et al., 2025; Narasimhan et al., 2025) (Fig. 2 B). Strikingly, among RORγt-lineage APCs, these markers are highly and specifically enriched in R-eTACs, supporting that these represent the same or similar populations. *Prdm16* in particular, which has been reported to have a functional role in RORγt APC-mediated oral tolerance (Fu et al., 2025), is exclusively expressed in R-eTACs among RORγt-lineage APCs, and shows the highest expression in R-eTAC2s and

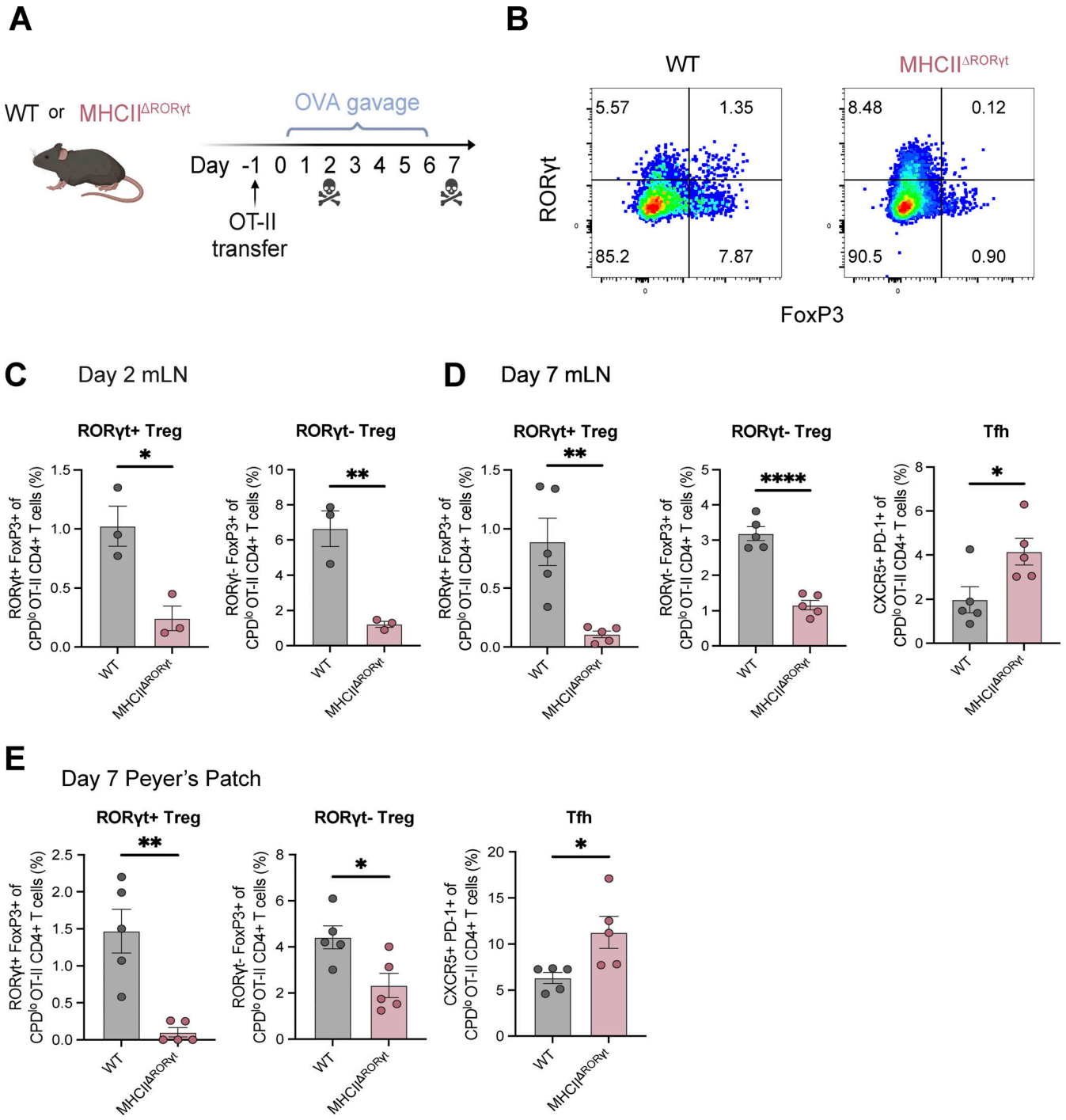

Figure 1. **RORγt-lineage APCs mediate oral tolerance to food antigen. (A)** Schematic of oral tolerance experimental design. Naïve OT-II cells were isolated from spleen and LNs (inguinal, axillary, and brachial) with magnetic column depletion. 0.5–1 × 10^6 cells were retro-orbitally transferred into WT or MHCII$^{\Delta RORγt}$ mice. 50 mg of OVA was gavaged at the indicated time points and harvested 2 or 7 days after first gavage. **(B and C)** Flow cytometry (B) and quantification of Cell Proliferation Dye (CPD)^{lo} OT-II (C) in WT and MHCII$^{\Delta RORγt}$ mLN after 2 days of oral OVA (n = 3 in each group). The bar graph shows RORγt$^+$ Treg (RORγt$^+$FoxP3$^+$) and RORγt$^-$ Treg (RORγt$^-$FoxP3$^+$). **(D)** Quantification of CPD^{lo} OT-II in WT and MHCII$^{\Delta RORγt}$ mLN after 7 days of oral OVA (n = 5 in each group). Tfh was gated as CXCR5$^+$PD1$^+$. **(E)** Quantification of CPD^{lo} OT-II in WT and MHCII$^{\Delta RORγt}$ PP after 7 days of oral OVA. Data in B–E are representative of two to three independent experiments. Error bars: mean ± SEM; statistics were calculated by unpaired two-sided t test; *P < 0.05, **P < 0.005, ****P < 0.0001.

R-eTAC3s (Fig. 2 B and Fig. S2 F). While distinct R-eTAC subpopulations have unique transcriptional signatures (Fig. 2 D and Table S1), they all share expression of *Aire* and this core gene set as well as transcriptional homology to both DCs (Fig. S2 G) and Aire-expressing medullary thymic epithelial cells (mTECs) (Fig. S2 H) as previously described (Wang et al., 2021).

We next carried out parallel characterization of RORγt-lineage MHCII$^+$ populations in early life (2-wk-old mice) by

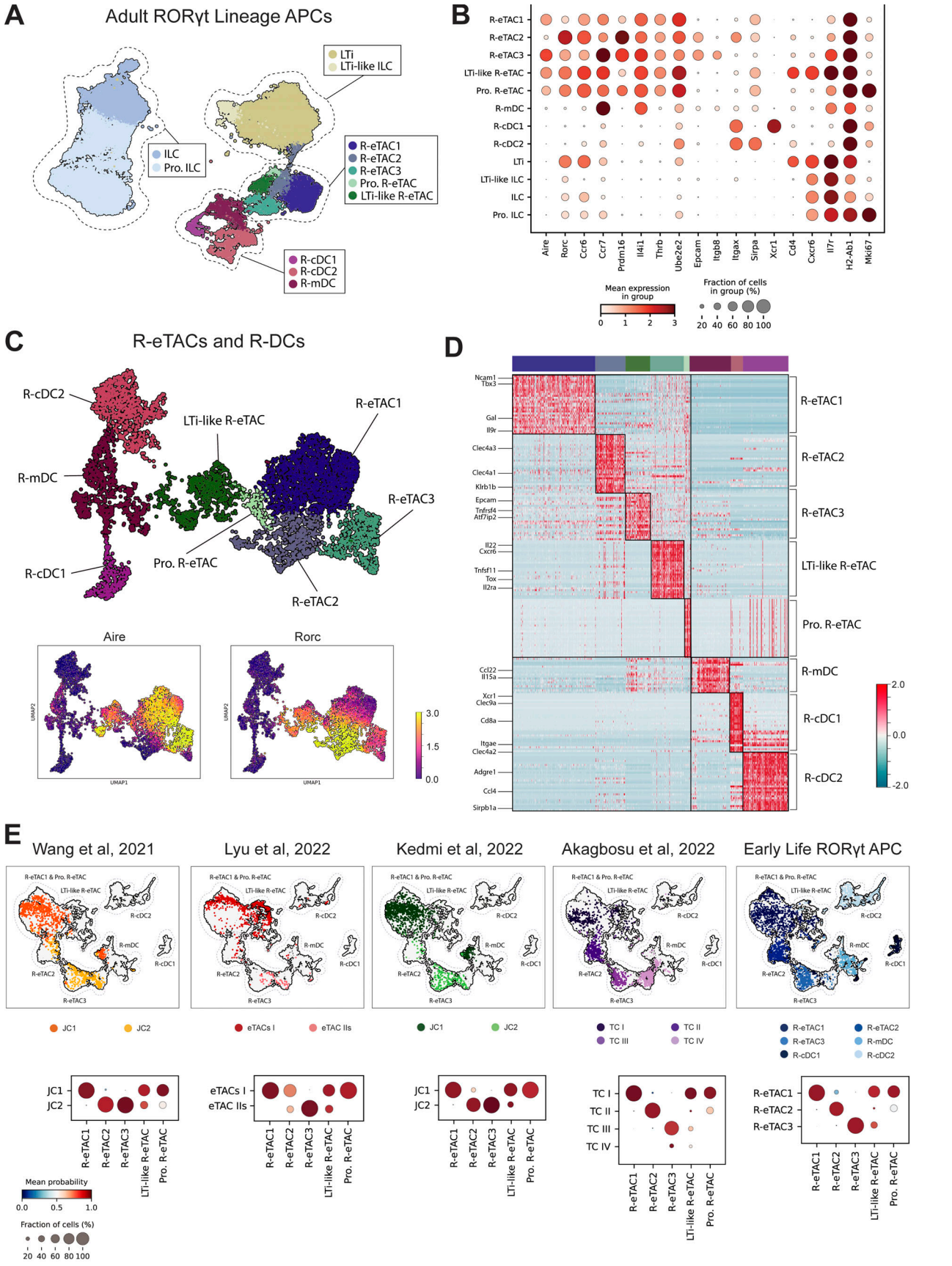

Figure 2. **Reconciling the diversity of RORγt-lineage APC populations. (A–D)** Spleen, mLN, and other LNs (cervical, inguinal, axillary, brachial, and para-aortic) from adult RORγt-lineage mice (*RORγt*^{Cre}×Rosa26-LSL-tdTmt) were harvested, digested, magnetically depleted of T and B cells, FACS-sorted (tdTmt^{+}

MHCII⁺), and subjected to single-cell sequencing. **(A)** Reduced dimensionality representation of our adult scRNA-seq data with annotated cell clusters. **(B)** Select gene expression in RORγt-lineage APC subsets. **(C)** Top: Reduced dimensionality representation of R-eTAC and R-DC subsets. Bottom: Gene expression of *Aire* and *Rorc* in those subsets. **(D)** Differential gene expression heatmap of RORγt-lineage APC subsets. **(E)** Top: Integrated UMAP of all available RORγt-lineage APC single-cell data, including Wang et al. (2021), Lyu et al. (2022a), Kedmi et al. (2022), Akagbosu et al. (2022), and our 2-wk-old data (left to right). Bottom: Corresponding CellTypist projections onto our adult scRNA-seq data.

scRNA-seq and found high concordance between these populations and their adult counterparts (Fig. 2 E, right and Fig. S2 I). Due to recent confusion around RORγt⁺ APCs, including varied nomenclature and sorting strategies, we next utilized single-cell variational inference (scVI) to merge and cluster all previously published single-cell data on RORγt⁺ APCs (Akagbosu et al., 2022; Kedmi et al., 2022; Lyu et al., 2022a; Wang et al., 2021) with our combined adult and 2-wk-old data. These merged data demonstrate high transcriptional homology across all datasets despite distinct sorting approaches, with R-eTAC1-3 corresponding closely to eTACs I/II, JC 1–3, and TC I–III. Only TC IV lacked concordance as this population was not found in our data or others (Fig. 2 E and Fig. S2 J).

Of note, our lineage-tracing approach uniquely captured R-DC subsets (R-cDC1, R-cDC2, and R-mDCs) in both our adult and early-life scRNA-seq data. These R-DCs were likely not captured in prior efforts using reporter- and not lineage-based approaches as they are *Aire*- and *Rorc*-negative. The presence of *tdTmt* transcript in these populations, while of lower frequency, suggests they are true RORγt-lineage APCs and not simply acquiring tdTomato protein secondarily, though we cannot rule out some contamination from secondary fluorophore acquisition. Thus, in summary we have identified ILCs/LTis, R-eTACs, and R-DCs as the principal populations of RORγt-lineage APCs in mouse SLOs, encompassing the landscape of putative populations responsible for the induction of oral tolerance.

R-eTACs are antigen-presenting cells of putative myeloid lineage

To validate the identity of these RORγt-lineage APC populations identified by scRNA-seq, and to specifically identify R-eTACs, we analyzed the previously described *RORγt*^{Cre}×*Aire*-GFP reporter×Rosa26-LSL-tdTmt mouse (Wang et al., 2021) by flow cytometry, which allows tracing of cells actively expressing Aire by GFP expression and all RORγt-lineage cells by tdTmt. We identified the major subsets of cells identified by our scRNA-seq data using the following gating strategy: ILCs/LTis (tdTmt⁺ MHCII⁺ CXCR6$^{\pm}$ CD90.2$^{\pm}$), R-eTAC1/3 (tdTmt⁺ MHCII⁺ CXCR6⁻ CD90.2⁻ CD11c^{lo}), R-eTAC2 (tdTmt⁺ MHCII⁺ CXCR6⁻ CD90.2⁻ CD11c^{hi} RORγt⁺), and R-DCs (tdTmt⁺ MHCII⁺ CXCR6⁻ CD90.2⁻ CD11c^{hi} RORγt⁻) (Fig. 3 A). Additionally, we found we could further dissect R-eTAC1s and R-eTAC3s based on EpCAM and CCR7 expression (Fig. S3 A) and R-DCs into R-cDCs and R-mDCs based on CCR7, XCR1, and SIRPα expression (Fig. S3 B), consistent with our scRNA-seq data. We were also able to validate intracellular Aire staining of eTACs by flow cytometry (Fig. S3 C) and further quantified the composition of Aire-GFP reporter and Aire protein positive cells out of all RORγt-lineage APCs. These data confirm that R-eTACs are the dominant population expressing both Aire reporter and protein (Fig. 3 B). Complementarily, we found that the majority of extrathymic Aire protein-expressing cells are of the RORγt lineage (Fig. 3 C) and express RORγt protein (Fig. S3 D). Our single-cell analysis showed that diverse R-eTAC subsets are present not just in the mLN, but also in the other SLOs (Fig. 3 D). We also validated this by flow cytometry, finding that by cell number, R-eTACs are most abundant in mesenteric and skin-draining LNs but present in all SLOs, supporting their potential tolerogenic roles in diverse tissues. Interestingly, the PP, siLP, and colonic lamina propria almost entirely lacked R-eTACs (Fig 3 E), though this does not exclude the presence of related, non-Aire-expressing R-eTACs in these sites (Fu et al., 2025). By gating GFP⁺ tdTmt⁺ cells from all pooled LNs, we found that R-eTACs are enriched in early life between 2 and 3 wk of age, decline moderately after weaning, but persist into late adulthood (Fig. S3 E), concordant with prior findings (Akagbosu et al., 2022).

Next, we sought to determine the antigen processing and presentation ability of R-eTACs by coculturing them with naïve OT-II and whole OVA protein. R-eTACs were sorted from SLOs as GFP⁺tdTmt⁺, along with control GFP⁻tdTmt⁻CD11c⁺ DC populations, and cocultured with whole OVA protein or OVA peptide for 72 h. R-eTACs were able to process and present OVA and induce OT-II proliferation to a similar extent as control GFP⁻ DCs (Fig. 3 F and Fig. S3 F), suggesting they function as bona fide APCs. Interestingly, R-eTACs also induced markedly higher frequency of FoxP3⁺ OT-II Tregs compared with DCs, supporting their putative tolerogenic capabilities (Fig. 3 G).

We have previously shown that R-eTACs are transcriptionally most similar to migratory DCs (Wang et al., 2021), but their hematopoietic lineage remains unclear. Indeed, extrathymic RORγt⁺Aire⁺ cells were first described as ILC3-like cells (Yamano et al., 2019), with potential interconversion between ILCs and R-eTACs suggested (Lyu et al., 2022b, *Preprint*). To determine whether R-eTACs share a lymphoid lineage with ILCs, we utilized *Il7r*$^{-/-}$ mice, which lack common lymphoid progenitors and fail to generate both lymphocytes and ILCs (Peschon et al., 1994). We generated mixed BMC mice with WT and *Il7r*$^{-/-}$ BM at a 1:2 ratio and quantified both lymphoid and myeloid cell subsets in the LNs 8 wk after reconstitution. As expected, *Il7r*$^{-/-}$ BM failed to give rise to ILCs but retained comparable proportions of DCs. Surprisingly, *Il7r*$^{-/-}$ BM also gave rise to normal proportions of R-eTACs, suggesting that this population is likely not of lymphoid lineage or does not pass through a common lymphoid progenitor stage, contrary to previous suggestions (Paucar Iza and Brown, 2024) (Fig. 3 H). By gating Aire⁺ R-eTAC1s and eTAC3s based on EpCAM and CCR7 staining, we further confirmed that *Il7r*$^{-/-}$ BM retains intact in R-eTAC subsets (Fig. S3 G). We independently confirmed these findings in a parallel mixed BMC model using *Rag2*$^{-/-}$*Il2rg*$^{-/-}$ mice, which also lack adaptive lymphocytes and ILCs (Cao et al.,

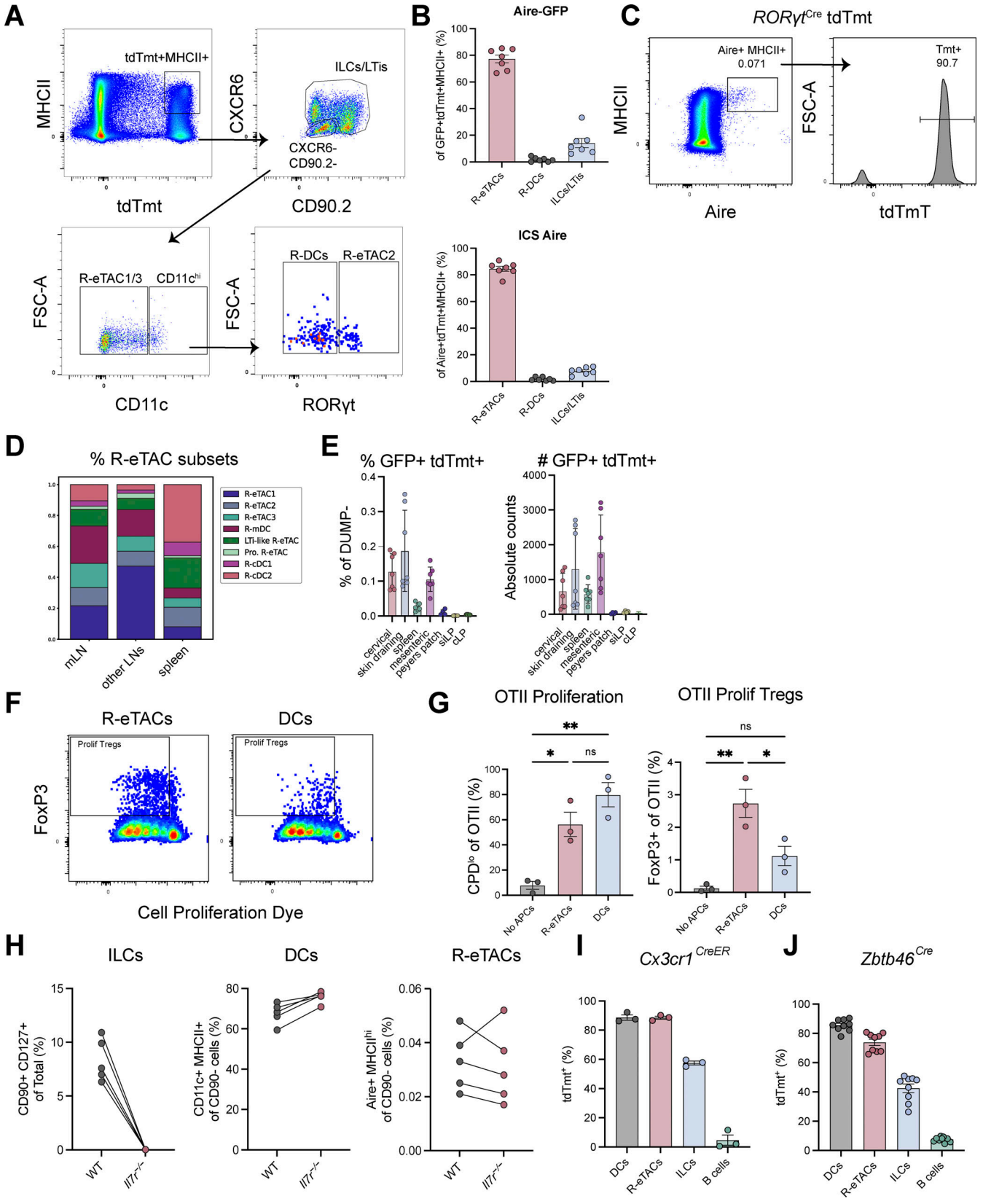

Figure 3. **R-eTACs are antigen-presenting cells of putative myeloid lineage. (A)** Flow cytometry plots showing the gating of R-eTAC1/3, R-eTAC2, R-DC, and ILCs/LTis isolated from LNs of RORγt-lineage tracing with *Aire* reporter mice (*RORγt*^{Cre}×*Aire*-GFP reporter×Rosa26-LSL-tdTmt). **(B)** Quantification of the composition of R-eTACs, R-DCs, and ILCs/LTis among Aire reporter (top) or Aire protein (bottom)-positive cells out of tdTmt$^+$MHCII$^+$ gate in the RORγt-lineage tracing with Aire reporter mice (n = 8). **(C)** Flow cytometry of cells isolated from LNs in RORγt lineage–tracing mice pre-gated on single, live, Lin$^-$ (SiglecF$^-$CD3$^-$B220$^-$Ly6G$^-$NK1.1$^-$F4/80$^-$). **(D)** Distribution of R-eTAC subsets across different organs in our adult scRNA-seq data. **(E)** Flow cytometry

quantification of percentage (left) and absolute count per mouse (right) of R-eTACs across different organs in RORγt lineage–tracing adult mice from Fig. 2 (n = 7). **(F)** Flow cytometry plots of OT-II proliferating Tregs (FoxP3$^+$CPD^{lo} of CD90.1$^+$CD90.2$^+$ T cells) after 72-h coculture with R-eTACs (GFP$^+$tdTmt$^+$) or DCs (GFP$^-$CD11c$^+$) isolated and sorted from mouse LNs. **(G)** Quantification of OT-II proliferation (CPD^{lo} of CD90.1$^+$CD90.2$^+$ T cells) and OT-II proliferating Tregs after coculture with no APCs, R-eTACs, or DCs (left to right) (n = 3 for each group). **(H)** Congenically distinct (CD45.2$^+$) BM cells were isolated from WT or *Il7r*$^{-/-}$ BM and mixed in 1:2 ratio and subsequently reconstituted in lethally irradiated recipient WT mice (CD45.1$^+$) to generate mixed BMCs. 8 wk after reconstitution, LNs (cervical, inguinal, axillary, brachial, mesenteric, and para-aortic) were isolated. Quantification of ILCs (CD90$^+$CD127$^+$), DCs (CD11c$^+$MHCII$^+$), and R-eTACs (Aire$^+$MHCII$^+$) from LNs of WT$^+$*Il7r*$^{-/-}$ mixed BMC mice (n = 5 for each group). **(I)** *Cx3cr1*^{CreER}×Rosa26-LSL-tdTmt mice were treated with tamoxifen three times a week for 4 wk for complete labeling. LNs were harvested, and tdTmt$^+$ cells were quantified by flow cytometry (n = 3). **(J)** LNs were harvested from adult *Zbtb46*^{Cre}×Rosa26-LSL-tdTmt mice, and tdTmt$^+$ cells were quantified by flow cytometry (n = 10). Data in C and H are representative of three independent experiments. Data in E are representative of two independent experiments. Data in B, C, F, G, I, and J are pooled from two to three independent experiments. Error bars: mean ± SEM; statistics were calculated by one-way ANOVA with Tukey's multiple comparisons test (G); *P < 0.05, **P < 0.005.

1995). Here again, ILCs were not found among the populations derived from the *Rag2*$^{-/-}$*Il2rg*$^{-/-}$ BM, while R-eTACs developed normally and showed no difference between WT and *Rag2*$^{-/-}$*Il2rg*$^{-/-}$ BM (Fig. S3 H). There was also no significant difference in R-eTAC1 and R-eTAC3 subsets between WT and *Rag2*$^{-/-}$*Il2rg*$^{-/-}$ BM (Fig. S3 I). Of note, the absolute number of R-eTACs, DCs, and all populations derived from *Il7r*$^{-/-}$ or *Rag2*$^{-/-}$*Il2rg*$^{-/-}$ BM was lower than the WT counterpart BM, suggesting an overall defect in homeostatic proliferation in the absence of signaling through these pathways.

Given the transcriptional homology between R-eTACs and migratory DCs (Akagbosu et al., 2022; Ulezko Antonova et al., 2023; Poliani et al., 2010; Wang et al., 2021), we next sought to address whether R-eTACs migrate to LNs in response to inflammation (Narasimhan et al., 2025). 24 h after neonatal gavage of TLR7/8 agonist R848, which has been shown to effectively induce DC migration (Yrlid et al., 2006), R-eTAC and DC percentages increased fourfold in the mLN, while ILCs did not change (Fig S3 J). To determine whether R-eTACs and DCs share common induction signals, we next administered recombinant Flt3L (rFlt3L) to WT mice, which induces expansion of DC progenitors (Maraskovsky et al., 1996; Waskow et al., 2008). Absolute numbers of DCs increased 30-fold after recombinant Flt3 administration, but interestingly, R-eTAC number did not change (Fig. S3 K). Conversely, treatment of WT mice with anti-Flt3L (αFlt3L) reduced DC cell numbers profoundly, but R-eTAC counts did not change (Fig. S3 L). These results suggest that R-eTACs do not share the Ftl3-Flt3L signaling requirements characteristic of conventional DCs.

To further map the putative myeloid lineage of R-eTACs, we used the *Cx3cr1*^{CreER}×Rosa26-LSL-tdTmt (Feng et al., 2022) and *Zbtb46*^{Cre} lineage-tracing systems (Loschko et al., 2016) and found that R-eTACs were labeled at similar percentages to DCs, while lymphocytes were not substantially traced (Fig. 3, I and J). Less than 5% of R-eTACs were traced by the *Clec9a*^{CreER}×Rosa26-LSL-tdTmt mouse (Schraml et al., 2013) (Fig. S3 M), in line with other groups' recent findings (Akagbosu et al., 2022; Narasimhan et al., 2025). While this potentially suggests a lineage unique from DCs, the precise relationship remains unclear. Lastly, the *Ms4a3*^{Cre}×Rosa26-LSL-tdTmt lineage tracer failed to label R-eTACs, suggesting they are not of a monocyte-derived lineage (Fig. S3 N). Thus, R-eTACs and their subsets can be identified through lineage tracing and intracellular Aire staining and function as tolerogenic APCs of a myeloid lineage. Overall, R-eTACs are distinct from ILCs, lymphocytes, and monocytes, while sharing some but not all characteristics of DCs.

R-eTACs mediate oral tolerance to food antigen

To determine whether ILC/LTis are required for diet-specific Treg induction, we next generated 1:2 mixed BMC mice from congenic MHCII$^{\Delta ROR\gamma t}$ and *Il7r*$^{-/-}$ donors. As *Il7r*$^{-/-}$ BM is deficient in all adaptive and ILCs but has intact R-eTACs (Fig. 3 H), mice with MHCII$^{\Delta ROR\gamma t}$ and *Il7r*$^{-/-}$ mixed BM lack all ILC/LTis as APCs but have functional antigen presentation from R-eTACs, as well as other myeloid populations (Fig. S4 A). By comparing MHCII$^{\Delta ROR\gamma t}$+*Il7r*$^{-/-}$ mixed BMCs with WT or MHCII$^{\Delta ROR\gamma t}$ BMCs, we can thus determine whether antigen presentation by nonlymphoid RORγt-lineage APCs is sufficient to rescue the loss of oral antigen-specific Tregs in MHCII$^{\Delta ROR\gamma t}$ mice (Fig. 4 A). Indeed, we found ILCs/LTis to be dispensable for oral tolerance induction, as MHCII$^{\Delta ROR\gamma t}$+*Il7r*$^{-/-}$ mixed BMC mice entirely rescued OT-II RORγt$^+$ and RORγt$^-$ Treg generation and restored Tfh percentages to similar levels of WT BMCs (Fig. 4 B). To measure the long-term impact of RORγt-lineage APC loss on oral tolerance, we next compared these mixed BMCs in an established mouse model of systemic delayed-type hypersensitivity (Esterházy et al., 2016; Hadis et al., 2011). After 8 wk of reconstitution, BMC mice were given OVA gavage on days 0 and 1, immunized with OVA in CFA on day 9, and received subcutaneous injections of OVA on days 23 and 33. Loss of tolerance was assessed by measuring serum IgG1 and IgG2c titers on day 35. MHCII$^{\Delta ROR\gamma t}$ BMC mice demonstrated robust anti-OVA IgG1 and IgG2c responses, which were entirely rescued by the presence of functional R-eTACs in MHCII$^{\Delta ROR\gamma t}$+*Il7r*$^{-/-}$ mixed BMC mice (Fig. 4 C). Finally, to map precisely which RORγt-lineage APCs are generated by *Il7r*-deficient BM, we crossed *Il7r*$^{-/-}$ mice to a RORγt-lineage tracer (*Il7r*$^{-/-}$×*RORγt*^{Cre}×Rosa26-LSL-tdTmt). We then generated congenic 1:2 mixed BMC mice in which both experimental and control donors carry the WT (no lineage tracer) BM plus either WT or *Il7r*-deficient RORγt lineage–traced BM. MHCII$^+$ tdTmt$^+$ cells from SLOs of both WT and *Il7r*$^{-/-}$ BM donors were sorted for scRNA-seq. Subsequent analysis revealed that all R-eTAC subsets were intact in this lineage and were in fact the predominant RORγt-lineage APC enriched in *Il7r*$^{-/-}$ BM (Fig. 4, D and E). While this approach does not exclude a potential role of RORγt-lineage DCs in oral tolerance, the dramatic enrichment of R-eTACs among RORγt-lineage APCs generated by *Il7r*-deficient BM, together with recent studies arguing

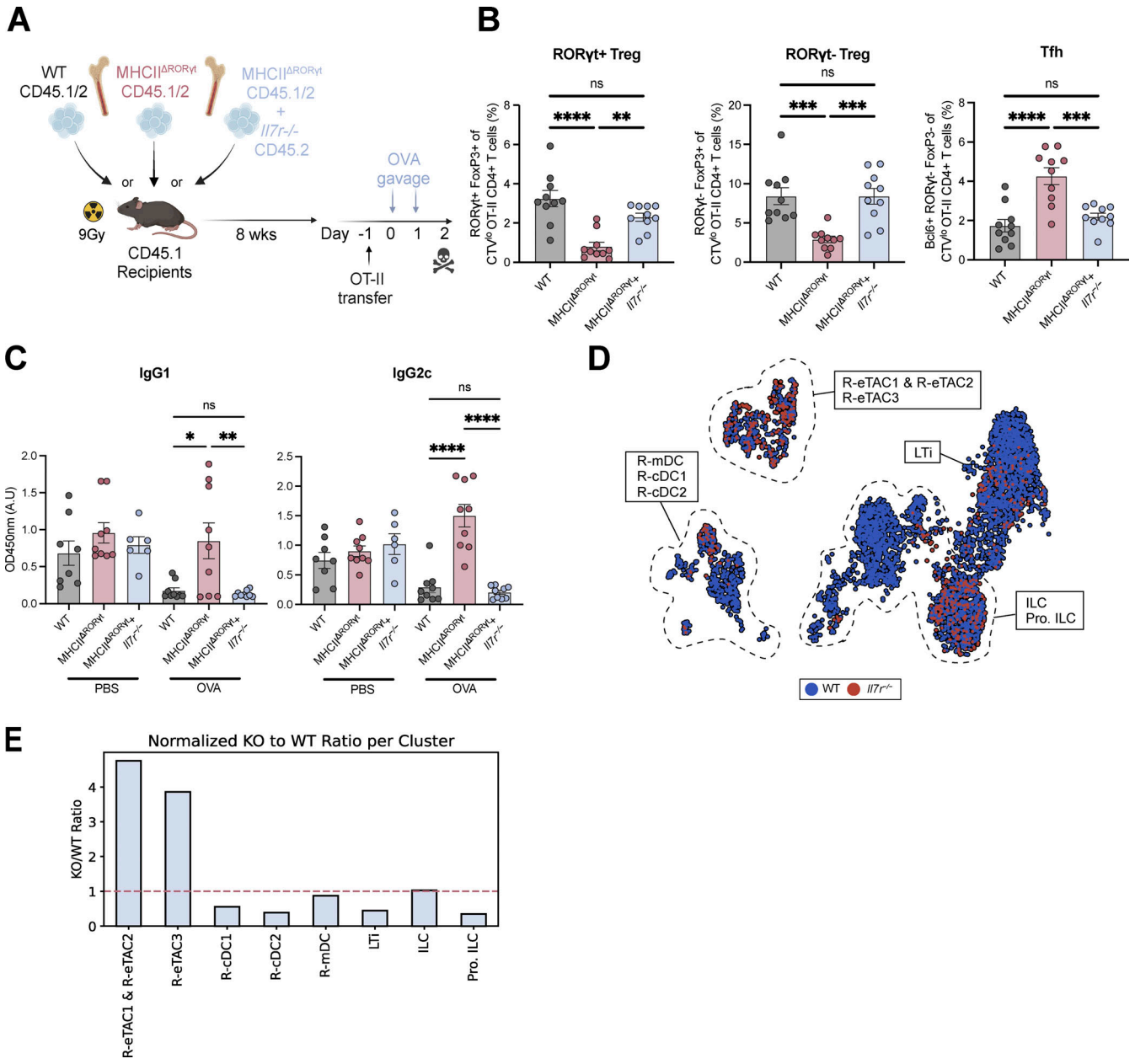

Figure 4. **ILCs are dispensable for oral tolerance to food antigen. (A)** Schematic of mixed BMC generation plus oral tolerance experimental design. Congenically distinct (CD45.2$^+$) BM cells were isolated from WT, MHCII$^{\Delta ROR\gamma t}$ *or Il7r*$^{-/-}$ BM and subsequently reconstituted in lethally irradiated recipient WT mice (CD45.1$^+$) to generate three groups of BMC mice: WT, MHCII$^{\Delta ROR\gamma t}$, and MHCII$^{\Delta ROR\gamma t}$+*Il7r*$^{-/-}$ (mixed in 1:2 ratio). 6–8 wk after reconstitution, mice were subjected to OT-II adoptive transfer and two OVA gavages. **(B)** Flow cytometry quantification of RORγt$^+$ Tregs, RORγt$^-$ Tregs, and Tfh out of CPD^{lo} OT-IIs in BMC mouse mLNs after 2 days of oral OVA (n = 10 from each group). **(C)** Quantification of OVA-specific IgG1 (left) and IgG2c (right) in serum isolated from mice subjected to a delayed-type hypersensitivity model (n = 10 from each group). The experimental design was as follows: reconstituted mice were gavaged with PBS (control) or tolerized with OVA (days 0–1), sensitized with subcutaneous CFA-OVA (day 9), challenged with subcutaneous OVA (days 23 and 33), and harvested for serum (day 35). **(D and E)** BM cells were isolated from congenically distinct CD45.2$^+$ *RORγt*^{Cre}×Rosa26-LSL-tdTmt (referred to as WT for simplicity) mice or *Il7r*$^{-/-}$×*RORγt*^{Cre}×Rosa26-LSL-tdTmt (*Il7r*$^{-/-}$) mice. These cells were then mixed at a 2:1 ratio with WT non–lineage-tracing CD45.1$^+$CD45.2$^+$ BM and transferred into lethally irradiated CD45.1$^+$ recipients. 8 wk after reconstitution, LN cells from WT or *Il7r*$^{-/-}$ mixed BMCs were isolated, sorted (tdTmt$^+$MHCII$^+$), and subjected to scRNA-seq. **(D)** UMAP from single-cell analysis of RORγt-lineage APCs present in WT and *Il7r*$^{-/-}$ mice. **(E)** Ratio (*Il7r* KO/WT) of different subsets of RORγt-lineage APCs from the single-cell analysis. Data in B and C are pooled from two independent experiments. Error bars: mean ± SEM; statistics were calculated by one-way ANOVA with Tukey's multiple comparisons test (B and C); *P < 0.05, **P < 0.005, ***P < 0.0005, ****P < 0.0001.

against a functional role of DCs in oral tolerance (Rudnitsky et al., 2024, *Preprint*), strongly supports a role of R-eTACs.

To more directly test whether R-eTACs are required for oral tolerance and the induction of dietary antigen-specific Tregs, we next utilized a previously described AireDTR mouse model, which, upon intraperitoneal administration of diphtheria toxin (DT), efficiently ablates Aire-expressing cells (Metzger et al., 2013) (Fig. 5 A and Fig. S4 B). Dose frequency was determined

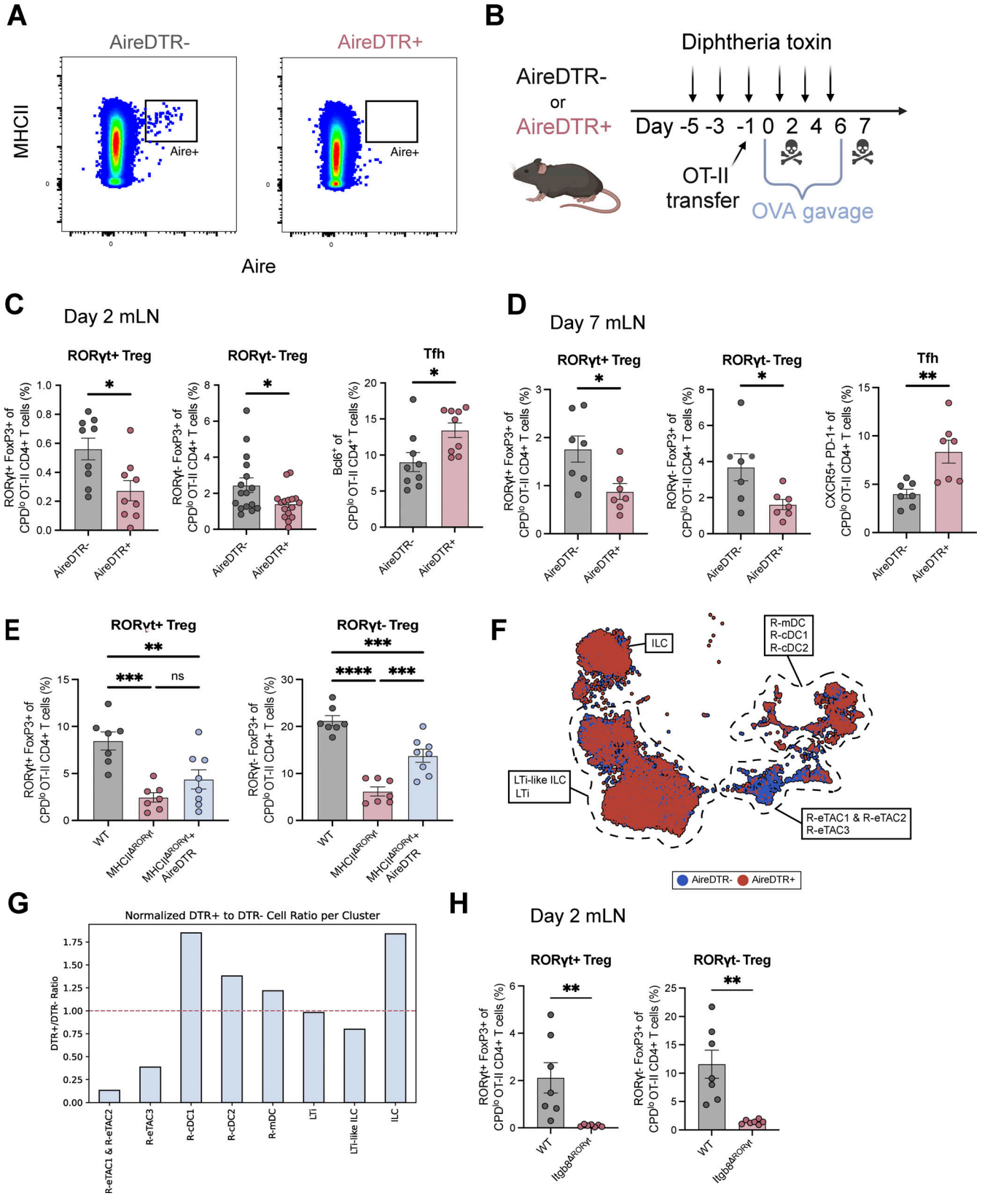

Figure 5. **R-eTACs mediate oral tolerance to food antigen. (A)** Flow cytometry of cells pre-gated on single, live, Lin⁻ from AireDTR⁻ and AireDTR⁺ mouse LNs. All mice were treated with DT every other day for five doses. **(B)** Schematic of AireDTR oral tolerance experimental design. AireDTR⁻ and AireDTR⁺ mice were pretreated with three doses of DT every other day to deplete Aire-expressing cells. After OT-II transfer and OVA gavage, mice are treated with three more doses of DT before harvest. **(C and D)** Quantification of RORγt⁺ Tregs, RORγt⁻ Tregs, and Tfh out of CPD^{lo} OT-IIs from AireDTR⁻ and AireDTR⁺ mLNs by flow cytometry after 2 days (n = 9 from each group) (C) and 7 days (n = 7 from each group) (D) of oral OVA. **(E)** Quantification of RORγt⁺ Tregs and RORγt⁻ Tregs out

of CPD^{lo} OT-IIs from mixed BMC generated from WT, MHCII$^{\Delta ROR\gamma t}$, and AireDTR mLN after 2 days of OVA gavage (n = 7 for WT and MHCII$^{\Delta ROR\gamma t}$, n = 8 for MHCII$^{\Delta ROR\gamma t}$+AireDTR). **(F and G)** BMCs were generated with either CD45.2$^+$ AireDTR$^-$×*RORγt*^{Cre}×Rosa26-LSL-tdTmt (herein referred to as AireDTR$^-$ for simplicity) or CD45.2$^+$ AireDTR$^+$×*RORγt*^{Cre}×Rosa26-LSL-tdTmt (AireDTR$^+$) mice. 8 wk after reconstitution, LN cells from AireDTR$^-$ and AireDTR$^+$ mixed BMCs were isolated, sorted (tdTmt$^+$MHCII$^+$), and subjected to scRNA-seq. DT was administered to all mice five times every other day before harvest. **(F)** UMAP from single-cell analysis of RORγt-lineage APCs present in AireDTR$^-$ and AireDTR$^+$ BMC mice after DT depletion. **(G)** Ratio (AireDTR$^+$/AireDTR$^-$) of different subsets of RORγt-lineage APCs from the single-cell analysis. **(H)** Oral tolerance experimental setup is the same as Fig. 1 A. Quantification of RORγt$^+$ Tregs and RORγt$^-$ Tregs out of CPD^{lo} OT-IIs isolated from mLN of WT versus Itgb8$^{\Delta ROR\gamma t}$ mice 2 days after OVA gavage (n = 7 from each group). Data in C, D, and H are pooled from two to three independent experiments. Data in E are representative of three independent experiments. Error bars: mean ± SEM; statistics were calculated by one-way ANOVA with Tukey's multiple comparisons test (E) and unpaired two-sided t test (C, D, and H); *P < 0.05, **P < 0.005, ***P < 0.0005, ****P < 0.0001.

based on pulse-chase experiments, which show a reconstitution half-life for R-eTACs of around 7 days (Fig. S4 C). To determine whether R-eTACs are necessary for oral tolerance, we first transferred naïve OT-II T cells into DT-treated AireDTR$^-$ or AireDTR$^+$ mice followed by 2–7 days of OVA gavage (Fig. 5 B). After 2 days of OVA gavage, AireDTR$^+$ mice had significantly decreased percentages of both OT-II RORγt$^+$ and RORγt$^-$ Tregs with an increased percentage of OT-II Tfh in the mLN (Fig. 5 C). AireDTR$^+$ mice harvested after 7 days of oral gavage had similarly diminished OT-II Tregs and elevated OT-II Tfh in the mLN and PP, as well as decreased anergic OT-IIs in the mLN compared to AireDTR$^-$ wild-type mice (Fig. 5 D and Fig. S4, D and E).

To assess whether Aire-expressing R-eTACs are required to rescue the loss of dietary antigen-specific Tregs observed in MHCII$^{\Delta ROR\gamma t}$ mice, we next generated mixed BMC with 1:1 MHCII$^{\Delta ROR\gamma t}$ and AireDTR BM (MHCII$^{\Delta ROR\gamma t}$ + AireDTR). 8 wk after reconstitution, we deleted R-eTACs in these mice by administering 6 doses of DT and compared them with non-BMC WT and MHCII$^{\Delta ROR\gamma t}$ controls. After 2 days of OVA feedings, BMC mice lacking R-eTACs as APCs (MHCII$^{\Delta ROR\gamma t}$ + AireDTR) had no rescue of RORγt$^+$ Tregs and only partial rescue of RORγt$^-$ Tregs (Fig. 5 E). This suggests R-eTACs are strictly necessary to induce OVA-specific RORγt$^+$ Tregs, while R-eTACs and other populations including R-DCs may participate in the induction of OVA-specific RORγt$^-$ Tregs. To precisely map which RORγt-lineage APCs are deleted in AireDTR mice, we next crossed the AireDTR transgene onto the RORγt-lineage tracer (AireDTR×*RORγt*^{Cre}×Rosa26-LSL-tdTmt), administered five doses of DT, and sorted tdTmt$^+$ MHCII$^+$ cells from mouse SLOs for scRNA-seq. Analysis revealed highly selective loss of all three R-eTAC subsets in these mice, while R-DCs and ILCs/LTis remained intact (Fig. 5, F and G). This selective deletion was further validated by flow cytometry (Fig. S4, F and G).

Of note, although extrathymic Aire expression in RORγt-lineage APCs has been shown to be important in the induction of Th17 cells in response to *Candida albicans* (Dobeš et al., 2022), Aire itself was dispensable for oral tolerance induction, as crossing Aire$^{fl/fl}$ mice with pan-hematopoietic *Vav1*^{iCre} (Aire$^{\Delta Vav1}$) or *RORγt*^{Cre} (Aire$^{\Delta ROR\gamma t}$) showed no defect in OT-II Treg generation (Fig. S5, A and B). Several groups have noted TGFβ-mediated Treg activation requires the expression of integrin αvβ8 by RORγt$^+$ APCs to induce commensal-specific Tregs (Akagbosu et al., 2022; Kedmi et al., 2022). We noted that R-eTACs, particularly R-eTAC3s, are highly enriched for integrin β8 (Fig. 2 B). Consistent with recent findings (Parisotto et al., 2024, *Preprint*), Itgb8$^{\Delta ROR\gamma t}$ mice showed a dramatic reduction in OVA-specific RORγt$^+$ and RORγt$^-$ Tregs in the mLN after 2 days of OVA feeding, which closely mirrors the results seen in MHCII$^{\Delta ROR\gamma t}$ mice (Fig. 5 H).

Taken together, these findings establish R-eTACs as a distinct, myeloid-derived APC with nonredundant roles in oral tolerance. By integrating scRNA-seq, lineage tracing, and functional studies, we demonstrate that R-eTACs, rather than ILCs, are essential for the induction of dietary antigen-specific Tregs and that R-eTACs are of myeloid and not lymphoid origin. The absence of R-eTACs disrupts Treg differentiation, facilitates Tfh differentiation, and ultimately leads to systemic failures of oral tolerance. Mechanistically, we identify *Itgb8*-mediated TGFβ activation as a key pathway through which R-eTACs facilitate immune tolerance.

Discussion

The ability to distinguish between pathogens and innocuous self- and commensal antigens is essential for maintaining gut homeostasis and overall health. Recent studies have established that RORγt$^+$ APCs contribute to immune tolerance by promoting peripheral Treg differentiation in response to commensal organisms, yet their role in oral tolerance to dietary antigens remains unclear. Of note, RORγt$^+$ APCs were shown to interact with dietary antigen-specific T cells through the LIPSTIC model, suggesting potential roles in priming dietary antigen-specific T cells (Campos Canesso et al., 2025). Here, we aimed to determine which RORγt-lineage APC populations are required for inducing dietary antigen-specific Tregs. Our findings reveal that RORγt-lineage APCs isolated from SLOs in mice comprise three main subsets: R-eTACs, ILCs/LTis, and R-DCs. We show that R-eTACs, but not ILC/LTis, are a major player in the process of oral tolerance induction against food antigens. Mice lacking functional antigen-presenting R-eTACs fail to generate antigen-specific Tregs and instead develop heightened antibody responses to dietary antigens. These findings establish R-eTACs as key mediators of oral tolerance and suggest potential targets for therapeutic modulation of immune tolerance.

Our scRNA-seq approach uniquely captured R-DCs and R-mDCs by utilizing a RORγtCre×Rosa26-LSL-tdTmt lineage tracer, rather than an active reporter. Unlike previous RORγt APC studies that labeled only actively expressing RORγ/RORγt, or Aire reporter populations, our lineage-tracing approach allowed us to identify and profile all cells that expressed or had expressed RORγt—a potentially more accurate landscape of the putative populations mediating the phenotypes observed in

these RORγt conditional knockout models. This enabled us to capture additional populations, such as those that have down-regulated *Aire* and *Rorc* expression over time, including some subsets of R-eTACs, R-cDCs, and R-mDCs. Interestingly, despite the diversity of sorting approaches and nomenclaures previously used to identify these populations, our data remained highly consistent with all prior approaches, and we show here that all prior efforts have largely identified the same R-eTAC populations. We thus define R-eTACs as a RORγt-lineage putatively myeloid-derived population enriched for *Aire* expression, with unique transcriptional homology to both DCs and medullary thymic epithelium, which are specifically depleted by DT in the AireDTR mouse model. This population is also likely the same as the recently described *Prdm16*$^{+}$ RORγt^{+} DCs (Narasimhan et al., 2025) and tolerogenic DCs (Fu et al., 2025) in both mouse and human, sharing a unique expression of key genes such as *Prdm16, Thrb, Il4i1*, and *Ube2e2*. The field will clearly benefit from some consensus around nomenclature as we continue to define the biology of these populations, but the data suggest we are all identifying the same or closely similar cell types.

We demonstrate here that R-eTACs are myeloid-derived and share several phenotypic and functional characteristics of DCs, but with some distinct features. Transcriptomic analyses reveal that R-eTACs exhibit gene expression signatures reminiscent of migratory DCs but are uniquely defined by Aire expression, a key regulator of immune tolerance more commonly associated with mTECs. Similar to DCs, R-eTACs do not derive from a lineage dependent on signaling from IL-7 or IL-2 common gamma cytokines. Instead, R-eTACs are tracked by *Cx3cr1*- and *Zbtb46*-lineage tracing similar to DCs, but not by *Ms4a3* monocyte-lineage tracers. Moreover, R-eTACs or their precursors appear to migrate to LNs upon TLR7/8 inflammatory stimulation, a feature characteristic of migratory DCs (Narasimhan et al., 2025). However, R-eTACs differ from DCs in critical ways: they are not traced by *Clec9a* lineage tracer, remain unresponsive to short-term Flt3L-driven expansion, and are resistant to short-term anti-Flt3L–driven depletion. While our work has not precisely mapped out the progenitors that give rise to R-eTACs, these findings highlight a distinct developmental pathway of R-eTACs within the myeloid lineage. Collectively, our data position R-eTACs as a specialized tolerogenic myeloid APC subset, one that, despite some functional overlap with DCs, plays a unique and nonredundant role in the maintenance of oral tolerance.

Our scRNA-seq analysis further reveals that all R-eTAC subsets are effectively ablated in our AireDTR model, while R-DCs remain fully intact. The partial rescue of RORγt- Tregs in MHCII$^{\Delta ROR\gamma t}$ + AireDTR mixed BMC compared with MHCII$^{\Delta ROR\gamma t}$ BMC mice suggests that R-eTACs alone are not sufficient to induce all food-specific Tregs and that other populations, such as R-DCs, may also contribute to RORγt^{-} OVA-specific Treg differentiation. However, preliminary findings from other groups using the MHCII-ON$^{\Delta Clec9a}$ mouse model revealed that cDCs alone cannot induce food antigen-specific Tregs (Rudnitsky et al., 2024, *Preprint*). This suggests that while R-eTACs are the primary drivers of oral tolerance, cDCs and R-DCs may play complementary roles, or that crosstalk between these populations may be relevant. Additionally, the transient deletion of R-eTACs in adult AireDTR mice may have different consequences for oral tolerance than the constitutive loss of antigen presentation in all RORγt-lineage APCs in MHCII$^{\Delta ROR\gamma t}$ mice, which lack these cells throughout early development.

Mechanistically, TGFβ signaling mediated by integrins αvβ8 from RORγt-lineage APCs—particularly R-eTACs and R-mDCs—plays a key role in inducing food antigen-specific peripheral Tregs, including both RORγt^{+} and RORγt^{-} subsets. In the absence of functional R-eTACs, OVA-specific naïve T cells become Tfh populations with increased frequency, and this crosstalk between R-eTACs and Tfh differentiation will be of interest for future studies, particularly related to the development of dietary antigen-specific antibody responses and allergy. R-eTACs do express high levels of ICOSL, and ICOS-ICOSL signaling plays critical roles in modulating Tfh and T follicular regulatory cell differentiation (Choi et al., 2011; Panneton et al., 2023; Stone et al., 2015). Beyond induction of dietary antigen-specific Tregs, our data also show that ∼40% of food antigen-specific T cells in WT mice lack lineage-defining transcription factors (such as Gata3, Tbet, FoxP3, and RORγt) and are phenotypically anergic (marked by CD73^{+} and FR4^{+}). These anergic T cells have also been implicated in overall tolerance to food antigens (Campos Canesso et al., 2025; Hong et al., 2022), and their proportion decreases markedly in mouse models with deficient RORγt APCs or R-eTACs. Further work may uncover additional mechanisms by which RORγt-lineage APCs contribute to overall induction of food antigen tolerance beyond induction of Tregs.

Recent studies identified *Prdm16* as a key transcription factor enriched in human-equivalent R-eTAC populations (Ulezko Antonova et al., 2023; Narasimhan et al., 2025). Another recent study further implicated *Prdm16* in regulating oral tolerance in RORγt-lineage APCs in mice (Fu et al., 2025). Consistent with these findings, we observed *Prdm16* expression to be highly specific to R-eTACs among RORγt-lineage APCs, with highest expression in R-eTAC2 and R-eTAC3 subsets. Given their co-expression of *Itgb8* and *Prdm16*, we hypothesize that R-eTAC2 and/or R-eTAC3 in particular may play key roles in tolerance to dietary antigens, but further studies are required to better define these lineage relationships and clarify the mechanisms by which these subsets enforce immune tolerance.

It is intriguing that RORγt-lineage APCs, recently implicated in regulating tolerance to commensal bacteria in the colon (Akagbosu et al., 2022; Kedmi et al., 2022; Lyu et al., 2022a), also appear critical for promoting tolerance to dietary antigens. Notably, TGFβ-mediated Treg differentiation plays a central role in both contexts. Whether the same tolerogenic mechanisms employed by RORγt-lineage APCs apply across these distinct antigen-delivery pathways, and in other disease contexts, remains to be determined. While some discrepant results may be attributable to differences in experimental approaches as well as the efficiency and specificity of various genetic tools, these differences may also reflect distinct roles of these populations in various contexts.

Emerging work suggests that the peri-weaning period is critical for the establishment of lifelong oral tolerance via Treg differentiation (Cheifetz and Knoop, 2024), and future research should explore the role of R-eTACs in this process. Our findings position R-eTACs as essential, putatively myeloid-derived mediators of gut homeostasis that are uniquely capable of modulating dietary antigen-specific T cell responses toward tolerance rather than inflammation. Therapeutically, a deeper understanding of tolerogenic RORγt-lineage APCs has significant implications for immune modulation. Oral tolerance has been proposed as a strategy for preventing and treating autoimmune diseases, including experimental autoimmune encephalomyelitis and type I diabetes (Pinheiro-Rosa et al., 2021; Weiner, 1997), and allograft tolerance (Wang et al., 2022). By defining R-eTAC identity and function, our study provides a foundation for future efforts to harness these populations as therapeutic targets for systemic immune modulation in autoimmunity, allograft tolerance, and allergic disease states.

Materials and methods

Mice

6- to 12-wk-old male or female mice were used for all the experiments in this study unless indicated. C57BL/6J (000664), CD45.1 (002014), CD90.1 (000406), OTII (004194), Rosa26-LSL-dtTmt (007914), *Aire*$^{fl/fl}$ (031409), *MHCII*$^{fl/fl}$ (037709), *RORγt*^{Cre} (022791), *Vav1*^{iCre} (008610), *Cx3cr1*^{CreER} (021160), *Zbtb46*^{Cre} (028538), and *Clec9a*^{CreER} (037804) were purchased from The Jackson Laboratory. Adig, AireDTR, and germline *Aire*$^{-/-}$ mice were generated and provided by the laboratory of Dr. Mark S. Anderson (University of California, San Francisco [UCSF], San Francisco, CA, USA), and were characterized as previously described (Anderson et al., 2002; Gardner et al., 2008; Metzger et al., 2013). *Il7r*$^{-/-}$ and *Rag2*$^{-/-}$*Il2rg*$^{-/-}$ mice were generously provided by Dr. Roberto R. Ricardo-Gonzalez (UCSF). *Itgb8*$^{fl/fl}$ mice (Proctor et al., 2005) were generously provided by Dr. Ari B. Molofsky (UCSF). *Ms4a3*^{Cre} was kindly provided by Dr. Amar Nijagal (UCSF). *Ms4a3*^{Cre} lineage–tracing mice were kindly provided by Dr. Martin Valdearcos (UCSF). Lineage-tracing mice were generated by crossing lineage-specific Cre with Rosa26-LSL-dtTmt. Congenically marked (CD90.1^{+}CD90.2^{+}) OTII mice were generated by crossing OTII mice to CD90.1 mice. All mice were housed in specific pathogen–free facilities at UCSF, and all animal studies were approved by the Institutional Committee on Animal Use and Care at UCSF. All mice were housed in a specific pathogen–free facility in a 12-h light/dark cycle with access to food and water ad libitum.

Mouse LN processing and purification

For scRNA-seq, mouse spleen, mesenteric, and other LNs (cervical, brachial, axillary, inguinal, and para-aortic) were procured and pooled in a digestion medium consisting of RPMI 1640 with 2% fetal bovine serum (FBS) (Sigma-Aldrich), with DNase I (100 µg/ml; Roche) and Liberase (96 µg/ml; Roche), minced and incubated at 37°C with gentle agitation for 30 min, and passed through a 70-µm filter. Adult samples only were resuspended for magnetic column enrichment (Miltenyi LS column depletion with Streptavidin or anti-biotin microbeads and biotinylated antibodies against B220, CD19, Ter119, TCRβ, and CD3ε). Cells were then sorted for live, tdTmt^{+}MHCII^{+} cells and processed for 10× single-cell analysis.

For eTAC characterization by flow cytometry, digested cells from LNs were resuspended for magnetic column enrichment (Miltenyi LS column depletion with anti-biotin microbeads and biotinylated antibodies against B220, Ter119, TCRβ, ± CD3ε). Cell viability and counts were evaluated with Vi-CELL XR (Beckman Coulter).

For OT-II characterization, mLNs or PP were procured, and cells were passed through a 70-µm cell strainer to achieve single-cell suspension for subsequent flow cytometry staining and analysis.

For siLP immune cell isolation, the small intestines were dissected out and the Peyers Patch's were removed. After cutting the intestines open longitudinally and cleaning out the intestinal contents, the small intestines were treated with 1× HBSS with 1 mM dithiothreitol for 10 min at room temperature (RT) and 3× with 5 mM EDTA in 1× HBSS supplemented with 5% FBS for 10 min at 37°C. Then, small intestines were minced and dissociated in digestion buffer (RPMI supplemented with 5% FBS) containing 1 mg/ml collagenase D (Roche), 100 µg/ml DNase I at 37°C for 30 min. Leukocytes were collected at a 40–80% Percoll gradient (GE Healthcare).

Antibodies and reagents

Fluorochrome- or biotin-conjugated antibodies against the following mouse targets were purchased from BD Biosciences: CD3e (145-2C11), B220 (RA3-6B2), Ly6G (1A8), EpCAM(G8.8), TCRβ (H57-5970), MHCII (AF6-120.1), CD8α (53-6.7), Bcl6 (K112-91), RORγt (Q31-378), CD90.1 (OX-7), Gata3 (L50-823); Thermo Fisher Scientific: Aire (5H12), SiglecF (1RNM44N), TCRβ (H57-597), CD3e (145-2C11), B220 (RA3-6B2), Ter119 (TER-119), CD19 (1D3), CD90.2 (30-H12), FoxP3 (FJK-16 s); and BioLegend: CD4 (GK1.5), NK1.1 (PK136), Ly6C (HK1.4), CD90.2 (30-H12), CD19 (6D5), F4/80 (BM8), CCR7 (4B12), MHCII (AF6-120.1), XCR1 (ZET), SIRPα (P84), TCRβ (GL3), CD45 (30-F11), CD73 (TY/11.8), FR4 (12A5), CD44 (IM7), CD45.2 (104), CD45.1 (A20), CXCR5 (L138D7), PD1 (29F.1A12), CXCR6 (SA051D1). Fc block (2.4G2) was purchased from BioXCell. Isotype control antibodies were purchased from the same source as target-specific antibodies. The Zombie NIR Fixable Viability Kit from BioLegend or DAPI was used for viability staining.

Flow cytometry staining

CCR7 antibody staining was done at 37°C for 20 min prior to live/dead staining (10 min, RT). Then, surface antibodies and Fc block were incubated with cells for 30 min at 4°C. For intracellular staining, cells were fixed and permeabilized with eBioscience FoxP3/Transcription Factor Fixation/Permeabilization solution, then washed with 1× permeabilization buffer before FoxP3 antibody incubation. For intracellular Aire staining, cells were fixed in 4% paraformaldehyde for 15 min at RT, then incubated with eBioscience FoxP3/Transcription Factor Fixation/Permeabilization solution (Thermo Fisher Scientific) for 30 min at 4°C. Cells were washed and resuspended in 1×

permeabilization buffer overnight at 4°C. The next day, intracellular antibody staining was incubated with cells in 1× permeabilization buffer for 1 h at RT. Finally, cells were washed in 1× permeabilization buffer and resuspended in the staining buffer for flow cytometry. Flow cytometry data were acquired on Cytek Aurora and analyzed using FlowJo (TreeStar v10.10.0). For eTACs gating, Lin$^-$ gate includes (SiglecF$^-$Ly6G$^-$NK1.1$^-$TCRβ$^-$B220$^-$F4/80$^-$).

BMC

CD45.1 BM recipients were irradiated with two doses of 450 rads (X-RAD 320; Precision X-Ray) 3–4 h apart before receiving 5–10 × 10^6 donor BM cells by retro-orbital injection. For mixed BMC experiments, congenically distinct donor BM cells were mixed 1:1 (in the case of MHCII$^{\Delta ROR\gamma t}$ + AireDTR) or 1:2 (in the case of MHCII$^{\Delta ROR\gamma t}$ + *Il7r*$^{-/-}$ to account of defect in homeostatic defect observed in *Il7r*$^{-/-}$ mice). Mice were allowed 6–8 wk for reconstitution before experimental use.

Adoptive T cell transfer

Single-cell suspension of lymphocytes was obtained from mashing LNs (inguinal, axillary, brachial) and spleen from TCR transgenic mice through a 70-µm cell strainer. Naïve CD4 T cells were isolated from OT-II TCR transgenic mice using the Naïve CD4 T cell Isolation Kit (130-104-453; Miltenyi Biotec). After magnetic column isolation, naïve T cells were stained with eBioscience Cell Proliferation Dye eFluor 450 (65-0842-90; Thermo Fisher Scientific) at 10 µM for 10 min at 37°C, then quenched with RPMI with 2% FBS. Labeled T cells were resuspended in HBSS without Ca^{2+} and Mg^{2+} before transferring into recipient mice by retro-orbital injections at 0.5–1 × 10^6 cells in 200 µl HBSS per mouse.

Oral OVA administration

OVA (grade III, A5378; Sigma-Aldrich) was administered orally using plastic gavage needles. For short-term oral tolerance experiments, OVA was gavaged 1 and 2 days after naïve OT-II adoptive transfer, at 50 mg in 200 µl PBS per mouse each day, and mice were sacrificed at 48 h after antigen exposure. For long-term oral OVA challenge, 50 mg in 200 µl PBS OVA was administered on days 1 and 2 after naïve OT-II transfer, and 25 mg in 100 µl PBS OVA on days 3–6 until experiment endpoint on day 7.

CFA-OVA immunization and subcutaneous challenge

CFA (263810; BD) and OVA in PBS were emulsified prior to injection for CFA-OVA immunization. 8 days after oral OVA administration, each mouse received 100 µl CFA and 300 µg endotoxin-free OVA (vac-pova-100; InvivoGen) dissolved in 100 µl PBS through subcutaneous injection between the shoulder blades. Antibody titer response was measured 24 days after CFA-OVA immunization.

DT administration

Mice were given DT (BML-G135-0001; Enzo) at 0.75 µg in 100 µl PBS by intraperitoneal injection on days −5, −3, −1, 1, 3, and 5, while OVA was administered orally on days 1 and 2.

Tamoxifen treatment

For induction of gene recombination in *Cx3cr1*^{CreER} mice, 30 mg/ml tamoxifen (T5648; Sigma-Aldrich) was dissolved in corn oil and administered 100 µl via oral gavage three times a week for 4 wk for complete labeling. Mice were harvested the day after the last tamoxifen treatment. For induction of gene recombination in *Clec9a*^{CreER} mice, mice were put on tamoxifen-containing chow (TD.130860; Inotiv) for a week before analysis.

R848 treatment

9- to 10-day-old mice were orally gavaged with 2–3 µg of R848 (InvivoGen) in PBS or PBS only as a control. mLNs were harvested and analyzed 24 h later.

Recombinant Flt3L and anti-Flt3L treatment

WT C57BL/6J mice were treated with 10 µg of either isotype (BE0096; BioXCell) or recombinant Flt3L (BE0098; BioXCell) for 7 days. Mice were sacrificed the next day, and LNs were harvested for subsequent flow analysis. Similarly, WT C57BL/6J mice were treated with 10 µg of either isotype (AB-1080C; R&D Systems) or anti-mouse Flt3L antibody (AF427; R&D Systems) for 7 days.

scRNA-seq

For experiments involving the adult and early-life RORγt-lineage tracing mice (RLT), scRNA-seq libraries were generated from pooled spleen, mLN, and other LN samples. For the *Il7r*$^{-/-}$ and AireDTR experiments, scRNA-seq libraries were generated from pooled LN samples from a given condition. Early-life samples were processed using 10x Genomics Chromium 3′ sequencing platform according to the manufacturer's protocols. The adult RLT, AireDTR, and *Il7r*$^{-/-}$ samples were processed using the 10x Genomics GEM-X 3′ sequencing platform according to the manufacturer's protocols performed by UCSF Genomics CoLab. The resulting libraries were sequenced on the Illumina NovaSeq 6000 performed by UCSF Genomics CoLab. The resulting libraries were sequenced on the Illumina NovaSeq 6000 through the UCSF Institute for Human Genetics and UCSF Center for Advanced Technology.

RLT scRNA-seq analyses

Adult RLT preprocessing

Raw sequencing reads were aligned to the mm10 reference genome using the standard Cell Ranger pipeline (Zheng et al., 2017). Cells were filtered out if they met any of the following criteria: >5% mitochondrial reads, >8,000 unique genes, and >60,000 total reads. The total cell counts sequenced are as follows: 20,629 (LN), 4,609 (mLN), 14,847 (spleen). The total cells postquality-control (QC) are as follows: 19,642 (LN), 4,135 (mLN), 13,222 (spleen).

Early-life RLT preprocessing

Raw sequencing reads were aligned as previously described. Cells were filtered out if they met any of the following criteria: >5% mitochondrial reads, >5,500 unique genes, and >35,000 total reads. The total cell counts sequenced are as follows:

17,975 (LN), 13,482 (mLN), 27,642 (spleen). The total cells post-QC are as follows: 14,682 (LN), 11,428 (mLN), 22,408 (spleen).

Analysis

The early-life and adult samples were separately analyzed in Python using the Scanpy package and scVI (Lopez et al., 2018) integration methodology. Briefly, each tissue sample (spleen, mLN, and other LNs) was restricted to the top jointly highly variable genes and combined. To impute gene expression in the combined dataset, a scVI model was trained on the combined data using tissue as the batch identifier, ribosomal gene percentage as a continuous covariate, and the negative binomial distribution of gene likelihood. Principal components and UMAP embedding were calculated from the scVI latent space. Clusters were identified using the Leiden algorithm. Clusters with low levels of *H2-ab1* and *Rorc* transcript were manually filtered out. Cell types were identified based on the expression of known marker genes. Three unique populations of putative R-eTACs were identified and termed R-eTAC1-3. The adult data also had two other R-eTAC populations: proliferating R-eTACs and LTi-like R-eTACs. Three unique populations of lineage-traced DCs were also identified in both adult and early-life datasets and termed R-cDC1, R-cDC2, and R-mDCs. Non-ILC, LTi, R-DC, or R-eTAC clusters are not shown. Batched corrected differentially expressed genes were called using scVI with a false discovery rate of 0.05. Units are displayed as a z-scored gene-level expression for heatmaps and scVI normalized expression for feature plots.

Il7r$^{-/-}$ and AireDTR scRNA-seq analyses

AireDTR preprocessing

Raw sequencing reads were aligned to the mm10 reference genome using the standard Cell Ranger pipeline (Zheng et al., 2017). Cells were filtered out if they met any of the following criteria: >3% mitochondrial reads, >8,000 unique genes, and >100,000 total reads. The total cell counts sequenced are as follows: 12,859 (DTR$^-$), 14,906 (DTR$^+$). The total cells post-QC and filtering are as follows: 9,234 (DTR$^-$), 8,510 (DTR$^+$).

Il7r$^{-/-}$ *preprocessing*

Raw sequencing reads were aligned as previously described. Cells were filtered out if they met any of the following criteria: >3% mitochondrial reads, >8,000 unique genes, and >100,000 total reads. The total cell counts sequenced are as follows: 7740 (WT), 784 (*Il7r*$^{-/-}$). The total cells post-QC and filtering are as follows: 4,387 (WT), 524 (*Il7r*$^{-/-}$).

Analysis

The *Il7r*$^{-/-}$ (WT and *Il7r*$^{-/-}$) and AireDTR (DTR$^-$ and DTR$^+$) experiments were separately analyzed in Python using the Scanpy package and scVI (Lopez et al., 2018) integration methodology. For a given experiment, samples from each condition were restricted to the top jointly highly variable genes and combined. To impute gene expression in our combined dataset, a scVI model was trained on the combined data using condition as the batch identifier and the negative binomial distribution of gene likelihood. Principal components and UMAP embedding were calculated from the scVI latent space. Clusters were identified using the Leiden algorithm. Clusters with low levels of *H2-ab1* and *Rorc* transcript were manually filtered. Cell types were identified based on the expression of known marker genes and Cell Typist label transfer (Xu et al., 2023) from our adult RLT dataset. Cell types that did not map to the adult RLT data are not shown. To calculate normalized ratios per cluster across conditions, the number of cells in a given cluster from a condition was divided by the total number of cells from that condition.

RORγt-lineage landscape integration

The Lyu et al. (2022a) (GSE184175), Kedmi et al. (2022) (GSE200147), and Akagbosu et al. (2022) (GSE174405) datasets were downloaded from the Gene Expression Omnibus. The Wang et al. (2021) (GSE176282) data were taken from our previous publications. For ease of integration, the integration was restricted to R-eTACs, R-DCs, and equivalent populations. Integration was performed in Python using methods detailed above, except the scVI model was trained using dataset source as a batch identifier and both MT gene percentage and ribosomal gene percentage were supplied as continuous covariates. Dimensionality reduction, clustering, and cell-type identification were performed in the same fashion as above. To validate our integration, CellTypist (Xu et al., 2023) was used to project cell-type labels from the Lyu et al. (2022a) and Akagbosu et al. (2022) datasets and our early-life dataset to our adult dataset.

APC and OT-II Coculture

Myeloid cells were obtained from digested LNs and spleen and isolated using magnetic column depletion from RORγt lineage–tracing mice (see digestion and purification method above). Lymphocyte-depleted samples were then FACS-sorted on single, live, CD19$^-$CD90.2$^-$, then GFP$^+$tdTmt$^+$ (R-eTACs), and GFP$^-$CD11c$^+$ (DCs). 3,500–6,500 APCs were then cocultured with Cell Proliferation Dye–labeled naïve OT-II T cells at a 1:10 ratio in the presence of either 100 µg/ml whole OVA protein or OVA$^{323-339}$ peptide (AS-27024; AnaSpec) for 72 h in a U-bottom 96-well plate. Culture media were made of RPMI with 10% FBS, 1× Pen/Strep/Glutamine, NEAA, HEPES, and β-mercaptoethanol.

ELISA

OVA (grade III, A5378; Sigma-Aldrich) was diluted in ELISA coating buffer (BioLegend) and coated on a high-bind half-area 96-well microplate (Corning) overnight at 4°C. After washing, wells were blocked with assay diluent (BioLegend) for 1 h at RT. Serum from mice, diluted in assay diluent, was incubated overnight at 4°C. After washing, wells were incubated with biotinylated anti-mouse IgG1 or IgG2c for 1 h at RT, followed by HRP Streptavidin (BioLegend) for 30 min at RT. Plates were developed with TMB substrate and stopped with STOP solution (BioLegend), and absorbance was measured at 450 nm.

Statistical analyses and visualization

All data points are shown in the graphs as mean value indicated and individual data points as shown. All statistical analyses were performed using GraphPad Prism (v10.2.3). Statistical

significance was calculated using one-way ANOVA with Tukey's multiple comparisons or the unpaired two-sided *t* test. *P < 0.05, **P < 0.005, ***P < 0.0005, and ****P < 0.0001 were considered significant. Experimental graphics were generated with BioRender (https://biorender.com/).

Online supplemental material

Fig. S1 presents data supporting Fig. 1, including the gating strategy, frequencies of Tfh and anergic OT-II T cells in mLN, phenotypes of endogenous T cells in MHCII$^{\Delta ROR\gamma t}$ mice, and the oral tolerance model in BMCs with either WT or MHCII$^{\Delta ROR\gamma t}$ donors. Fig. S2 supports Fig. 2, showing additional feature plots, frequencies of tdTmt$^+$, GFP$^+$, and Aire-expressing cells, ImmGen-based similarity scores, and analysis of early-life RORγt-lineage APCs. Fig. S3 supports Fig. 3 with flow cytometry gating for RORγt-lineage APC subsets, Aire flow validation, and lineage-tracing experiments. Fig. S4 provides additional data for Figs. 4 and 5, including validation and kinetics of knockout or DT depletion, oral tolerance phenotypes in mLN and PP, and gating strategies confirming DT depletion in RORγt-lineage APCs. Fig. S5 shows that Aire is dispensable in RORγt-lineage APC-mediated oral tolerance to dietary antigens. Table S1 lists differentially expressed genes from adult RORγt lineage–traced mice.

Data availability

All data necessary to understand and evaluate the conclusions of this paper are provided in the manuscript and supplementary materials. The sequencing data underlying Fig. 2 A, Fig. 4 D, Fig. 5 F, and Fig. S2 I were generated for this manuscript and are openly available in the Gene Expression Omnibus (GEO) under the following accession numbers: GSE273746 (adult RLT), GSE291696 (*Il7r*$^{-/-}$), GSE291411 (AireDTR), and GSE285182 (early-life RLT). The data underlying Fig. 2 E are from publicly available datasets in GEO with the following accession numbers: GSE184175, GSE174405, GSE176282, GSE200147. Source data are provided in this manuscript.

Acknowledgments

We thank all members of Gardner and Anderson laboratories for their helpful discussions. We also thank Drs. Mark Anderson, Dan Littman, and Ranit Kedmi for their feedback and insight. We thank Vinh Nguyen and other members of the UCSF Parnassus Flow Cytometry CoLab for technical support. We also thank Annie Poon and Catherine Chu of the UCSF Genomics CoLab, Charina Julian of the UCSF Institute for Human Genetics, and members of Center for Advanced Technology for their technical support on single-cell sequencing. Sequencing was performed at the UCSF Center for Advanced Technology, supported by UCSF Program in Breakthrough Biomedical Research, Research Resource Program International Medical Informatics Association, and National Institutes of Health 1S10OD028511-01 grants.

This work is supported by the National Institutes of Health grant R01 AI145858 (J.M. Gardner), National Institutes of Health training grant 5T32AI007334 (I.-H. Sun), National Institute of Health predoctoral fellowship 1F31AI172348 (J. Wang), National Institute of Health predoctoral fellowship 1F31CA288017 (M.P. Arvedson), National Institute of Health Medical Scientist Training Program training grant 5T32GM141323 (A.E. Qualls), Achievement Rewards for College Scientists Fellowship (J. Wang, J. Germino), Pew Biomedical Scholars Program (J.M. Gardner), Burroughs Wellcome Fund (J.M. Gardner), Parker Institute for Cancer Immunotherapy (J.M. Gardner), and W.M. Keck Foundation (J.M. Gardner).

Author contributions: I.-H. Sun: conceptualization, formal analysis, investigation, methodology, validation, visualization, and writing—original draft, review, and editing. A.E. Qualls: conceptualization, formal analysis, investigation, methodology, validation, visualization, and writing—original draft, review, and editing. H.S. Yin: conceptualization, formal analysis, investigation, visualization, and writing—review and editing. J. Wang: conceptualization, data curation, formal analysis, investigation, methodology, resources, validation, visualization, and writing—original draft, review, and editing. M.P. Arvedson: investigation. J. Germino: data curation, formal analysis, and writing—review and editing. N.K. Horner: formal analysis, investigation, and validation. S. Zhong: investigation and resources. J. Du: investigation and resources. M. Valdearcos: resources. V. Ntranos: methodology and supervision. R.M. Locksley: methodology, resources, supervision, and writing—review and editing. R.R. Ricardo-Gonzalez: resources and writing—review and editing. J.M. Gardner: conceptualization, data curation, funding acquisition, methodology, project administration, resources, supervision, validation, visualization, and writing—review and editing.

Disclosures: R.M. Locksley reported other from Genentech outside the submitted work. No other disclosures were reported.

Submitted: 17 March 2025
Revised: 10 April 2025
Accepted: 14 April 2025

References

Abramson, J., J. Dobeš, M. Lyu, and G.F. Sonnenberg. 2023. The emerging family of RORγt+ antigen-presenting cells. *Nat. Rev. Immunol.* 24:64–77. https://doi.org/10.1038/s41577-023-00906-5

Akagbosu, B., Z. Tayyebi, G. Shibu, Y.A. Paucar Iza, D. Deep, Y.F. Parisotto, L. Fisher, H.A. Pasolli, V. Thevin, R. Elmentaite, et al. 2022. Novel antigen-presenting cell imparts Treg-dependent tolerance to gut microbiota. *Nature*. 610:752–760. https://doi.org/10.1038/s41586-022-05309-5

Anderson, M.S., E.S. Venanzi, L. Klein, Z. Chen, S.P. Berzins, S.J. Turley, H. von Boehmer, R. Bronson, A. Dierich, C. Benoist, and D. Mathis. 2002. Projection of an immunological self shadow within the thymus by the aire protein. *Science*. 298:1395–1401. https://doi.org/10.1126/science.1075958

Campos Canesso, M.C., T.B.R. de Castro, S. Nakandakari-Higa, A. Lockhart, J. Luehr, J. Bortolatto, R. Parsa, D. Esterházy, M. Lyu, T.T. Liu, et al. 2025. Identification of antigen-presenting cell-T cell interactions driving immune responses to food. *Science*. 387:eado5088. https://doi.org/10.1126/science.ado5088

Cao, X., E.W. Shores, J. Hu-Li, M.R. Anver, B.L. Kelsall, S.M. Russell, J. Drago, M. Noguchi, A. Grinberg, E.T. Bloom, et al. 1995. Defective lymphoid development in mice lacking expression of the common cytokine receptor gamma chain. *Immunity*. 2:223–238. https://doi.org/10.1016/1074-7613(95)90047-0

Cheifetz, T.R., and K.A. Knoop. 2024. The right educational environment: Oral tolerance in early life. *Immunol. Rev.* 326:17–34. https://doi.org/10.1111/imr.13366

Chen, Y., J.I. Inobe, R. Marks, P. Gonnella, V.K. Kuchroo, and H.L. Weiner. 1995. Peripheral deletion of antigen-reactive T cells in oral tolerance. *Nature*. 376:177–180. https://doi.org/10.1038/376177a0

Choi, Y.S., R. Kageyama, D. Eto, T.C. Escobar, R.J. Johnston, L. Monticelli, C. Lao, and S. Crotty. 2011. ICOS receptor instructs T follicular helper cell versus effector cell differentiation via induction of the transcriptional repressor Bcl6. *Immunity*. 34:932–946. https://doi.org/10.1016/j.immuni.2011.03.023

Coombes, J.L., K.R.R. Siddiqui, C.V. Arancibia-Cárcamo, J. Hall, C.M. Sun, Y. Belkaid, and F. Powrie. 2007. A functionally specialized population of mucosal CD103+ DCs induces Foxp3+ regulatory T cells via a TGF-β and retinoic acid-dependent mechanism. *J. Exp. Med.* 204:1757–1764. https://doi.org/10.1084/jem.20070590

Dobeš, J., O. Ben-Nun, A. Binyamin, L. Stoler-Barak, B.E. Oftedal, Y. Goldfarb, N. Kadouri, Y. Gruper, T. Givony, I. Zalayat, et al. 2022. Extrathymic expression of Aire controls the induction of effective TH17 cell-mediated immune response to Candida albicans. *Nat. Immunol.* 23:1098–1108. https://doi.org/10.1038/s41590-022-01247-6

Dunlop, J.H., and C.A. Keet. 2018. Epidemiology of food allergy. *Immunol. Allergy Clin. North Am.* 38:13–25. https://doi.org/10.1016/j.iac.2017.09.002

Esterházy, D., J. Loschko, M. London, V. Jove, T.Y. Oliveira, and D. Mucida. 2016. Classical dendritic cells are required for dietary antigen–mediated induction of peripheral Treg cells and tolerance. *Nat. Immunol.* 17:545–555. https://doi.org/10.1038/ni.3408

Esterházy, D., M.C.C. Canesso, L. Mesin, P.A. Muller, T.B.R. de Castro, A. Lockhart, M. ElJalby, A.M.C. Faria, and D. Mucida. 2019. Compartmentalized gut lymph node drainage dictates adaptive immune responses. *Nature*. 569:126–130. https://doi.org/10.1038/s41586-019-1125-3

Feng, J., J.N. Pucella, G. Jang, M. Alcántara-Hernández, S. Upadhaya, N.M. Adams, A. Khodadadi-Jamayran, C.M. Lau, M. Stoeckius, S. Hao, et al. 2022. Clonal lineage tracing reveals shared origin of conventional and plasmacytoid dendritic cells. *Immunity*. 55:405–422.e11. https://doi.org/10.1016/j.immuni.2022.01.016

Friedman, A., and H.L. Weiner. 1994. Induction of anergy or active suppression following oral tolerance is determined by antigen dosage. *Proc. Natl. Acad. Sci. USA*. 91:6688–6692. https://doi.org/10.1073/pnas.91.14.6688

Fu, L., R. Upadhyay, M. Pokrovskii, F.M. Chen, G. Romero-Meza, A. Griesemer, and D.R. Littman. 2025. Prdm16-dependent antigen-presenting cells induce tolerance to gut antigens. *Nature*. 40228524. https://doi.org/10.1038/s41586-025-08982-4

Gardner, J.M., J.J. Devoss, R.S. Friedman, D.J. Wong, Y.X. Tan, X. Zhou, K.P. Johannes, M.A. Su, H.Y. Chang, M.F. Krummel, and M.S. Anderson. 2008. Deletional tolerance mediated by extrathymic Aire-expressing cells. *Science*. 321:843–847. https://doi.org/10.1126/science.1159407

Gardner, J.M., T.C. Metzger, E.J. McMahon, B.B. Au-Yeung, A.K. Krawisz, W. Lu, J.D. Price, K.P. Johannes, A.T. Satpathy, K.M. Murphy, et al. 2013. Extrathymic Aire-expressing cells are a distinct bone marrow-derived population that induce functional inactivation of CD4$^+$ T cells. *Immunity*. 39:560–572. https://doi.org/10.1016/j.immuni.2013.08.005

Garkaby, J., L. Epov, N. Musallam, M. Almog, E. Bamberger, A. Mandelberg, I. Dalal, and A. Kessel. 2021. The sesame-peanut conundrum in Israel: Reevaluation of food allergy prevalence in young children. *J. Allergy Clin. Immunol. Pract.* 9:200–205. https://doi.org/10.1016/j.jaip.2020.08.010

Hadis, U., B. Wahl, O. Schulz, M. Hardtke-Wolenski, A. Schippers, N. Wagner, W. Müller, T. Sparwasser, R. Förster, and O. Pabst. 2011. Intestinal tolerance requires gut homing and expansion of FoxP3+ regulatory T cells in the lamina propria. *Immunity*. 34:237–246. https://doi.org/10.1016/j.immuni.2011.01.016

Hepworth, M.R., L.A. Monticelli, T.C. Fung, C.G.K. Ziegler, S. Grunberg, R. Sinha, A.R. Mantegazza, H.L. Ma, A. Crawford, J.M. Angelosanto, et al. 2013. Innate lymphoid cells regulate CD4+ T-cell responses to intestinal commensal bacteria. *Nature*. 498:113–117. https://doi.org/10.1038/nature12240

Hepworth, M.R., T.C. Fung, S.H. Masur, J.R. Kelsen, F.M. McConnell, J. Dubrot, D.R. Withers, S. Hugues, M.A. Farrar, W. Reith, et al. 2015. Immune tolerance. Group 3 innate lymphoid cells mediate intestinal selection of commensal bacteria-specific CD4$^+$ T cells. *Science*. 348:1031–1035. https://doi.org/10.1126/science.aaa4812

Hong, S.W., P.D. Krueger, K.C. Osum, T. Dileepan, A. Herman, D.L. Mueller, and M.K. Jenkins. 2022. Immune tolerance of food is mediated by layers of CD4+ T cell dysfunction. *Nature*. 607:762–768. https://doi.org/10.1038/s41586-022-04916-6

Kedmi, R., T.A. Najar, K.R. Mesa, A. Grayson, L. Kroehling, Y. Hao, S. Hao, M. Pokrovskii, M. Xu, J. Talbot, et al. 2022. A RORγt+ cell instructs gut microbiota-specific Treg cell differentiation. *Nature*. 610:737–743. https://doi.org/10.1038/s41586-022-05089-y

Lopez, R., J. Regier, M.B. Cole, M.I. Jordan, and N. Yosef. 2018. Deep generative modeling for single-cell transcriptomics. *Nat. Methods*. 15:1053–1058. https://doi.org/10.1038/s41592-018-0229-2

Loschko, J., H.A. Schreiber, G.J. Rieke, D. Esterházy, M.M. Meredith, V.A. Pedicord, K.H. Yao, S. Caballero, E.G. Pamer, D. Mucida, and M.C. Nussenzweig. 2016. Absence of MHC class II on cDCs results in microbial-dependent intestinal inflammation. *J. Exp. Med.* 213:517–534. https://doi.org/10.1084/jem.20160062

Lyu, M., H. Suzuki, L. Kang, F. Gaspal, W. Zhou, J. Goc, L. Zhou, J. Zhou, W. Zhang, D. Artis, et al. 2022a. ILC3s select microbiota-specific regulatory T cells to establish tolerance in the gut. *Nature*. 610:744–751. https://doi.org/10.1038/s41586-022-05141-x

Lyu, M., H. Suzuki, L. Kang, F. Gaspal, W. Zhou, J. Goc, L. Zhou, J. Zhou, W. Zhang, J.R.I.L.C. Bank, et al. 2022b. ILC3s select for RORγt+ Tregs and establish tolerance to intestinal microbiota. *bioRxiv*. https://doi.org/10.1101/2022.04.25.489463 (Preprint posted April 26, 2022).

Maraskovsky, E., K. Brasel, M. Teepe, E.R. Roux, S.D. Lyman, K. Shortman, and H.J. McKenna. 1996. Dramatic increase in the numbers of functionally mature dendritic cells in Flt3 ligand-treated mice: Multiple dendritic cell subpopulations identified. *J. Exp. Med.* 184:1953–1962. https://doi.org/10.1084/jem.184.5.1953

Mazzini, E., L. Massimiliano, G. Penna, and M. Rescigno. 2014. Oral tolerance can be established via gap junction transfer of fed antigens from CX3CR1$^+$ macrophages to CD103$^+$ dendritic cells. *Immunity*. 40:248–261. https://doi.org/10.1016/j.immuni.2013.12.012

Metzger, T.C., I.S. Khan, J.M. Gardner, M.L. Mouchess, K.P. Johannes, A.K. Krawisz, K.M. Skrzypczynska, and M.S. Anderson. 2013. Lineage tracing and cell ablation identify a post-Aire-expressing thymic epithelial cell population. *Cell Rep.* 5:166–179. https://doi.org/10.1016/j.celrep.2013.08.038

Narasimhan, H., M.L. Richter, R. Shakiba, N.E. Papaioannou, C. Stehle, K. Ravi Rengarajan, I. Ulmert, A. Kendirli, C. de la Rosa, P.Y. Kuo, et al. 2025. RORγt-expressing dendritic cells are functionally versatile and evolutionarily conserved antigen-presenting cells. *Proc. Natl. Acad. Sci. USA*. 122:e2417308122. https://doi.org/10.1073/pnas.2417308122

Pabst, O., and A.M. Mowat. 2012. Oral tolerance to food protein. *Mucosal Immunol.* 5:232–239. https://doi.org/10.1038/mi.2012.4

Panneton, V., B.C. Mindt, Y. Bouklouch, A. Bouchard, S. Mohammaei, J. Chang, N. Diamantopoulos, M. Witalis, J. Li, A. Stancescu, et al. 2023. ICOS costimulation is indispensable for the differentiation of T follicular regulatory cells. *Life Sci. Alliance*. 6:e202201615. https://doi.org/10.26508/lsa.202201615

Parisotto, Y.F., V. Cabric, T. Park, B. Akagbosu, Z. Zhao, Y. Lo, L. Fisher, G. Shibu, Y.A.P. Iza, C. Leslie, and C.C. Brown. 2024. Thetis cells induce food-specific Treg cell differentiation and oral tolerance. *bioRxiv*. https://doi.org/10.1101/2024.05.08.592952 (Preprint posted May 10, 2024).

Paucar Iza, Y.A., and C.C. Brown. 2024. Early life imprinting of intestinal immune tolerance and tissue homeostasis. *Immunol. Rev.* 323:303–315. https://doi.org/10.1111/imr.13321

Peschon, J.J., P.J. Morrissey, K.H. Grabstein, F.J. Ramsdell, E. Maraskovsky, B.C. Gliniak, L.S. Park, S.F. Ziegler, D.E. Williams, C.B. Ware, et al. 1994. Early lymphocyte expansion is severely impaired in interleukin 7 receptor-deficient mice. *J. Exp. Med.* 180:1955–1960. https://doi.org/10.1084/jem.180.5.1955

Pinheiro-Rosa, N., L. Torres, M.A. Oliveira, M.F. Andrade-Oliveira, M.A.F. Guimarães, M.M. Coelho, J.L. Alves, T.U. Maioli, and A.M.C. Faria. 2021. Oral tolerance as antigen-specific immunotherapy. *Immunother. Adv.* 1:ltab017. https://doi.org/10.1093/immadv/ltab017

Poliani, P.L., K. Kisand, V. Marrella, M. Ravanini, L.D. Notarangelo, A. Villa, P. Peterson, and F. Facchetti. 2010. Human peripheral lymphoid tissues contain autoimmune regulator-expressing dendritic cells. *Am. J. Pathol.* 176:1104–1112. https://doi.org/10.2353/ajpath.2010.090956

Proctor, J.M., K. Zang, D. Wang, R. Wang, and L.F. Reichardt. 2005. Vascular development of the brain requires beta8 integrin expression in the neuroepithelium. *J. Neurosci.* 25:9940–9948. https://doi.org/10.1523/JNEUROSCI.3467-05.2005

Rudnitsky, A., H. Oh, J. Talmor, and R. Kedmi. 2024. Coordinated network of T cells and antigen presenting cells regulate tolerance to food. *bioRxiv*. https://doi.org/10.1101/2024.07.11.603064 (Preprint posted July 16, 2024).

Schraml, B.U., J. van Blijswijk, S. Zelenay, P.G. Whitney, A. Filby, S.E. Acton, N.C. Rogers, N. Moncaut, J.J. Carvajal, C. Reis e Sousa, and E. Sousa. 2013. Genetic tracing via DNGR-1 expression history defines dendritic cells as a hematopoietic lineage. *Cell*. 154:843–858. https://doi.org/10.1016/j.cell.2013.07.014

Stone, E.L., M. Pepper, C.D. Katayama, Y.M. Kerdiles, C.Y. Lai, E. Emslie, Y.C. Lin, E. Yang, A.W. Goldrath, M.O. Li, et al. 2015. ICOS coreceptor signaling inactivates the transcription factor FOXO1 to promote Tfh cell differentiation. *Immunity*. 42:239–251. https://doi.org/10.1016/j.immuni.2015.01.017

Ulezko Antonova, A., S. Lonardi, M. Monti, F. Missale, C. Fan, M.L. Coates, M. Bugatti, N. Jaeger, P. Fernandes Rodrigues, S. Brioschi, et al. 2023. A distinct human cell type expressing MHCII and RORγt with dual characteristics of dendritic cells and type 3 innate lymphoid cells. *Proc. Natl. Acad. Sci. USA*. 120:e2318710120. https://doi.org/10.1073/pnas.2318710120

Vale, S.L., M. Lobb, M.J. Netting, K. Murray, R. Clifford, D.E. Campbell, and S.M. Salter. 2021. A systematic review of infant feeding food allergy prevention guidelines - can we AGREE? *World Allergy Organ. J.* 14:100550. https://doi.org/10.1016/j.waojou.2021.100550

Wang, J., C.A. Lareau, J.L. Bautista, A.R. Gupta, K. Sandor, J. Germino, Y. Yin, M.P. Arvedson, G.C. Reeder, N.T. Cramer, et al. 2021. Single-cell multiomics defines tolerogenic extrathymic Aire-expressing populations with unique homology to thymic epithelium. *Sci. Immunol.* 6:eabl5053. https://doi.org/10.1126/sciimmunol.abl5053

Wang, P., L. Chen, C.M. McIntosh, J.I. Lane, R. Li, S.Z. Xie, H. Sattar, D. Esterhazy, A.S. Chong, and M.L. Alegre. 2022. Oral alloantigen exposure promotes donor-specific tolerance in a mouse model of minor-mismatched skin transplantation. *Am. J. Transpl.* 22:2348–2359. https://doi.org/10.1111/ajt.17107

Waskow, C., K. Liu, G. Darrasse-Jèze, P. Guermonprez, F. Ginhoux, M. Merad, T. Shengelia, K. Yao, and M. Nussenzweig. 2008. The receptor tyrosine kinase Flt3 is required for dendritic cell development in peripheral lymphoid tissues. *Nat. Immunol.* 9:676–683. https://doi.org/10.1038/ni.1615

Weiner, H.L. 1997. Oral tolerance for the treatment of autoimmune diseases. *Annu. Rev. Med.* 48:341–351. https://doi.org/10.1146/annurev.med.48.1.341

Worbs, T., U. Bode, S. Yan, M.W. Hoffmann, G. Hintzen, G. Bernhardt, R. Förster, and O. Pabst. 2006. Oral tolerance originates in the intestinal immune system and relies on antigen carriage by dendritic cells. *J. Exp. Med.* 203:519–527. https://doi.org/10.1084/jem.20052016

Xu, C., M. Prete, S. Webb, L. Jardine, B.J. Stewart, R. Hoo, P. He, K.B. Meyer, and S.A. Teichmann. 2023. Automatic cell-type harmonization and integration across Human Cell Atlas datasets. *Cell*. 186:5876–5891.e20. https://doi.org/10.1016/j.cell.2023.11.026

Yamano, T., J. Dobeš, M. Vobořil, M. Steinert, T. Brabec, N. Ziętara, M. Dobešová, C. Ohnmacht, M. Laan, P. Peterson, et al. 2019. Aire-expressing ILC3-like cells in the lymph node display potent APC features. *J. Exp. Med.* 216:1027–1037. https://doi.org/10.1084/jem.20181430

Yrlid, U., S.W. Milling, J.L. Miller, S. Cartland, C.D. Jenkins, and G.G. MacPherson. 2006. Regulation of intestinal dendritic cell migration and activation by plasmacytoid dendritic cells, TNF-alpha and type 1 IFNs after feeding a TLR7/8 ligand. *J. Immunol.* 176:5205–5212. https://doi.org/10.4049/jimmunol.176.9.5205

Zheng, G.X.Y., J.M. Terry, P. Belgrader, P. Ryvkin, Z.W. Bent, R. Wilson, S.B. Ziraldo, T.D. Wheeler, G.P. McDermott, J. Zhu, et al. 2017. Massively parallel digital transcriptional profiling of single cells. *Nat. Commun.* 8:14049. https://doi.org/10.1038/ncomms14049

JEM

Supplemental material

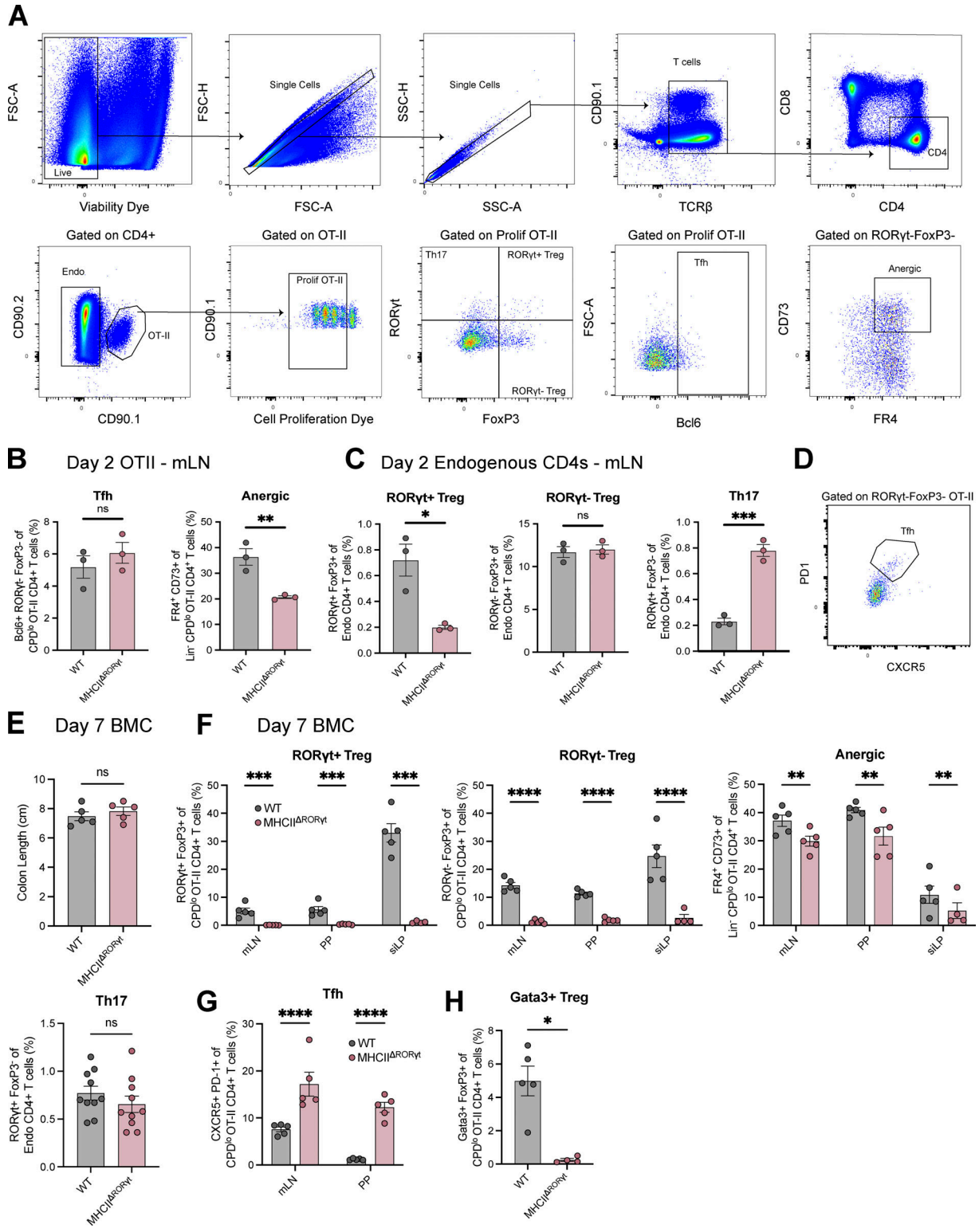

Figure S1. **RORγt-lineage APCs drive the induction of tolerance to dietary protein.** Related to Fig. 1. **(A)** Gating strategy for endogenous T cells and OVA-specific T cells (OT-II) from the mLN. **(B)** Quantification of Tfh (Bcl6$^+$FoxP3$^-$RORγt$^-$) and anergic (FR4$^+$CD73$^+$) OT-IIs in the mLN after 2 days of OVA gavage (n = 3 from each group). **(C)** Quantification of RORγt$^+$ Tregs (RORγt$^+$FoxP3$^+$), RORγt$^-$ Tregs (RORγt$^-$FoxP3$^+$), and Th17 (RORγt$^+$ FoxP3$^-$) from endogenous CD4 T cell subsets in the mLN after 2 days of OVA gavage (n = 3 from each group). **(D)** Gating strategy for OT-II Tfh (CXCR5$^+$PD1$^+$) in the mLN and PP for 7-day oral OVA experiments. **(E–H)** WT and MHCII$^{\Delta RORγt}$ BM cells were reconstituted in CD45.1 congenic hosts. 8 wk after reconstitution, the experiment was performed similar to Fig. 1 A (n = 5 from each group). **(E)** Colon length (top) and quantification of endogenous Th17 in the mLN (bottom) from WT and MHCII$^{\Delta RORγt}$ BMC mice. **(F)** Quantification of RORγt$^+$ Tregs, RORγt$^-$ Treg, and anergic OT-II in the mLN, PP, and siLP after 7 days of oral OVA. **(G)** Quantification of Tfh OT-II in the mLN and PP. **(H)** Quantification of Gata3$^+$ Treg OT-II in siLP. Data in B and C are representative of two independent experiments. Data in E–H are one experiment. Error bars: mean ± SEM; statistics were calculated by an unpaired two-sided t test; *P < 0.05, **P < 0.005, ***P < 0.0005, ****P < 0.0005.

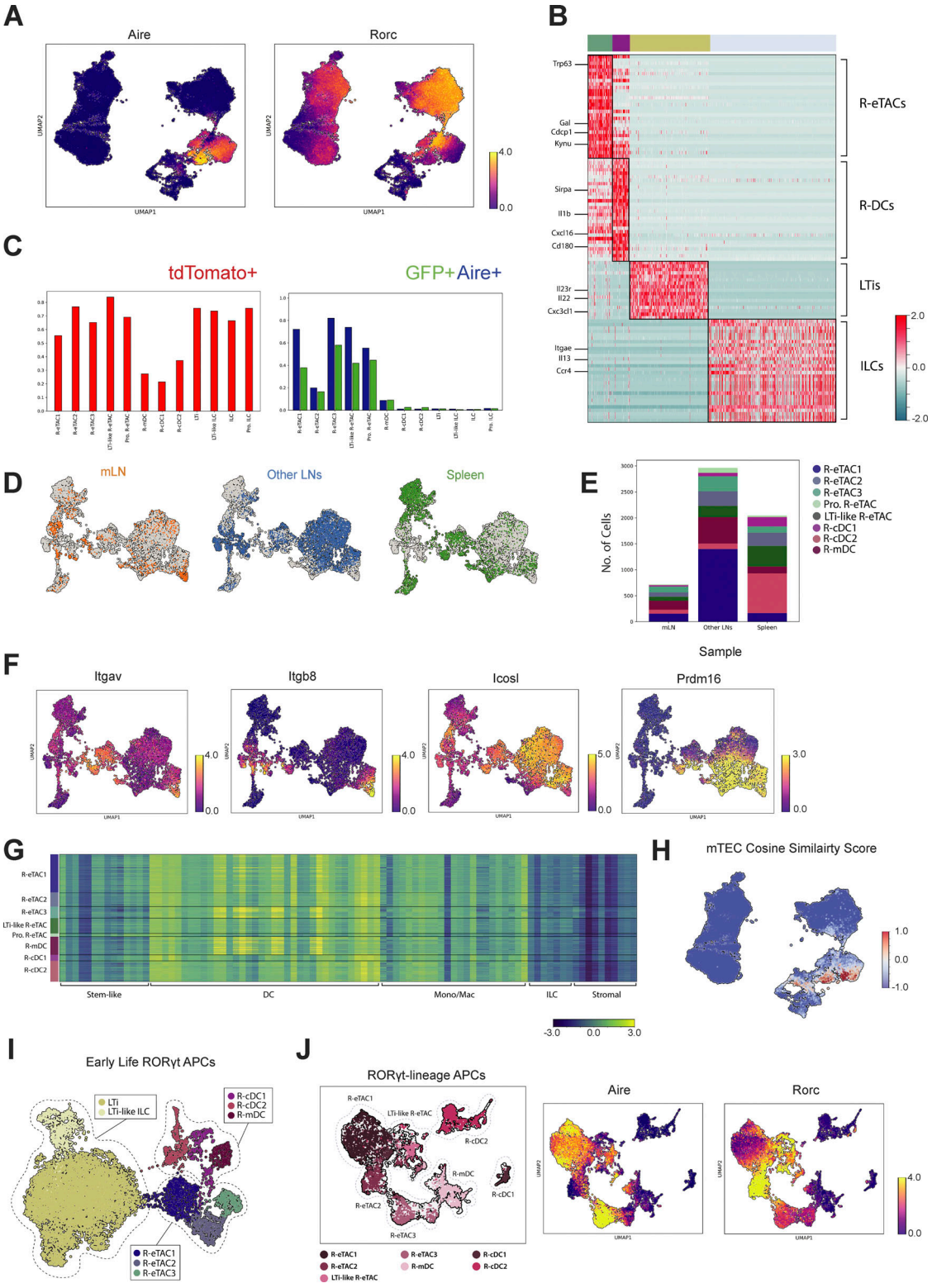

Figure S2. **Defining the heterogeneity of RORγt-lineage APC subsets.** Related to Fig. 2. **(A)** Expression of *Aire* and *Rorc* in adult tdTmt⁺MHCII⁺ scRNA-seq clusters. **(B)** Heatmap with differential gene expression of cell clusters from scRNA-seq data. **(C)** tdTomato (left), as well as *Aire*-GFP and *Aire* transcript (right) expression levels across RORγt-lineage APC clusters. **(D)** Distribution of R-eTAC subset clusters found from each sample origin: mLN, spleen, and other LNs (labeled UMAP to reference is Fig. 2 C). **(E)** Number of cells among R-eTAC subset clusters found in each sample origin. **(F)** Expression of *Itgav*, *Itgb8*, *Icosl*, and *Prdm16* in adult scRNA-seq clusters. **(G)** Heatmap showing similarities between R-eTAC clusters to other immune cell clusters from ImmGen. **(H)** Similarity score between adult RORγt-lineage APC clusters and mTECs. **(I)** Reduced dimensionality representation of scRNA-seq data with annotated cell clusters in 2-wk-old mice. **(J)** Integrated UMAP of all available RORγt-lineage APC single-cell data, displaying our adult scRNA-seq data (left), as well as expression of *Aire* and *Rorc* across the integrated scRNA-seq clusters (middle and right).

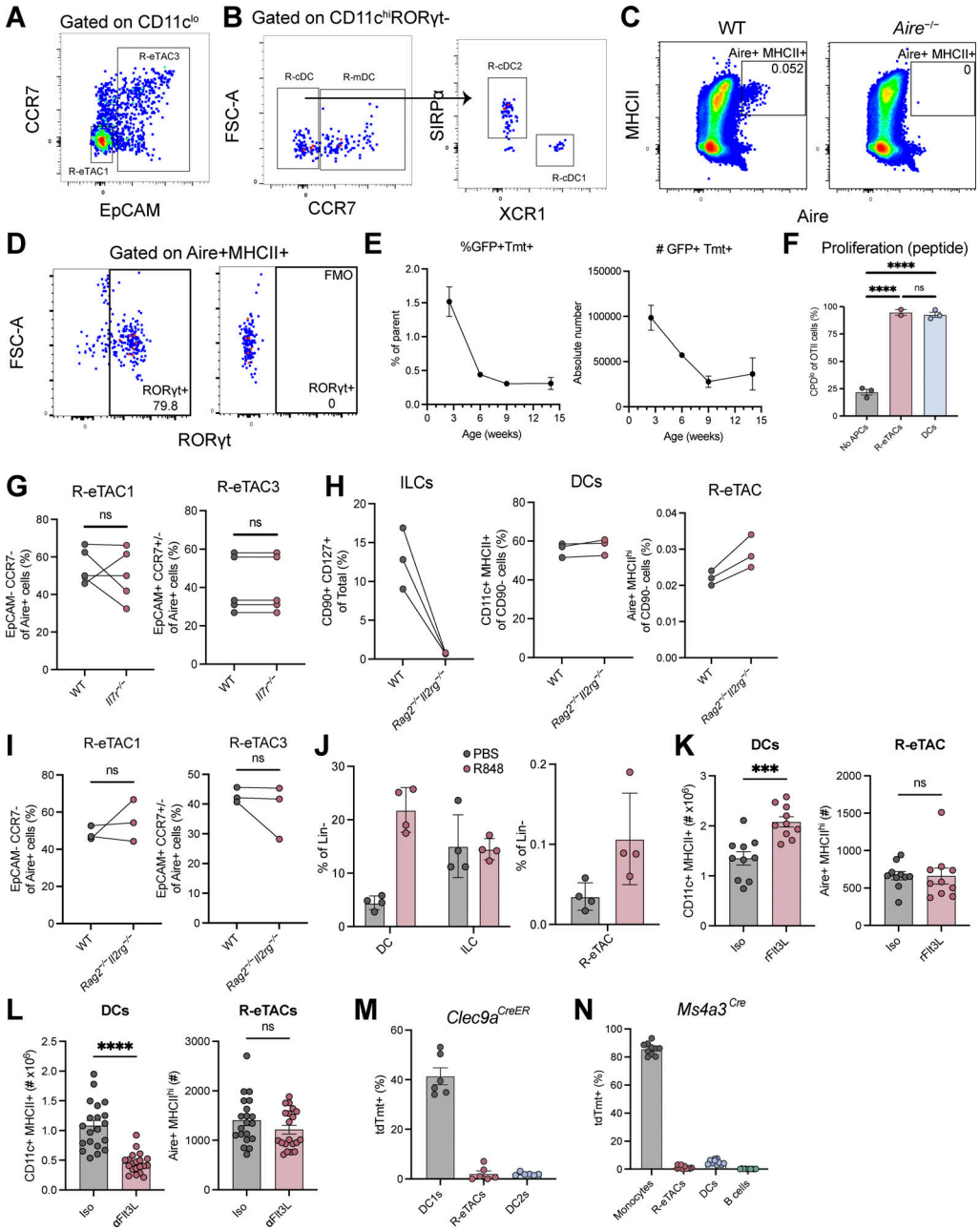

Figure S3. **R-eTACs represent a putatievly myeloid population with characteristics distinct from DCs.** Related to Fig. 3. **(A)** Flow cytometry plot showing the gating of R-eTAC1s (EpCAM⁻CCR7⁻) and R-eTAC3s (EpCAM⁺). This gating is from the R-eTAC1/3 shown in Fig. 3 A. **(B)** Flow cytometry plots showing the gating of R-mDCs (CCR7⁺), R-cDC1s (XCR1⁺SIRPα⁻), and R-cDC2s (XCR1⁻SIRPα⁺) from the R-DC shown in Fig. 3 A. **(C)** Flow cytometry validation of intracellular Aire staining between WT and germline *Aire*$^{-/-}$ mice. **(D)** Flow cytometry plots of intracellular RORγt staining on the MHCII⁺Aire⁺ cells. **(E)** Flow cytometry quantification of GFP⁺tdTmt⁺ percentage of parent (left) and absolute counts per mouse (right) from all pooled LNs from RORγt lineage–tracing mice with Aire reporter at various ages, gated on single, live, Lin⁻ cells (n = 3). **(F)** Quantification of the proliferation of OT-II cells cocultured with R-eTACs (GFP⁺tdTmt⁺) versus DCs (GFP⁻CD11c⁺) in the presence of OVA peptide after 72 h. **(G)** Experimental setup similar to Fig. 3 H. Quantification of R-eTAC subsets from the Aire⁺MHCII⁺ cells in the *Il7r*$^{-/-}$ or WT-derived portions of the BM (n = 5). **(H and I)** Experimental setup similar to Fig. 3 H, except with *Rag2*$^{-/-}$ *Il2rg*$^{-/-}$ BM cells instead of *Il7r*$^{-/-}$. Quantification of ILCs (CD90.2⁺CD127⁺), DCs (CD11c⁺MHCII⁺), and R-eTACs (Aire⁺MHCII⁺) (H) and R-eTAC subsets (I) from LNs of *Rag2*$^{-/-}$ *Il2rg*$^{-/-}$ mixed BMC mice (n = 3). **(J)** Quantification of DCs, ILCs, and R-eTACs from LNs of neonatal mice gavaged once with PBS or R848 and harvested 24 h later (n = 4 from each group, each dot is pooled from three mice). **(K)** WT mice were intraperitoneally treated with either isotype (Iso) or recombinant Flt3L (rFlt3L) for 7 days. DCs and R-eTACs were quantified from LNs (n = 10 from each group). **(L)** WT mice were intraperitoneally treated with either isotype (Iso) or anti-Flt3L antibody (αFlt3L) for 7 days. DCs and R-eTACs were quantified from the spleen (n = 20 from each group). **(M)** Flow cytometry quantification of DC subsets and R-eTACs from *Clec9a*^{CreER}×Rosa26-LSL-tdTmt mice LNs (n = 6). Mice were put on tamoxifen chow for 1 wk to induce labeling. **(N)** Flow cytometry quantification of monocytes, R-eTACs, DCs, and B cells from *Ms4a3*^{Cre}×Rosa26-LSL-tdTmt mouse LNs (n = 10). Data in E are from one independent experiments. Data in F–I are representative of at least three independent experiments. Data in J–N are pooled from two to three independent experiments. Error bars: mean ± SEM; statistics were calculated by one-way ANOVA with Tukey's multiple comparisons test (F) or unpaired two-sided t test (G–I, K, and L); ***P < 0.0005, ****P < 0.0001.

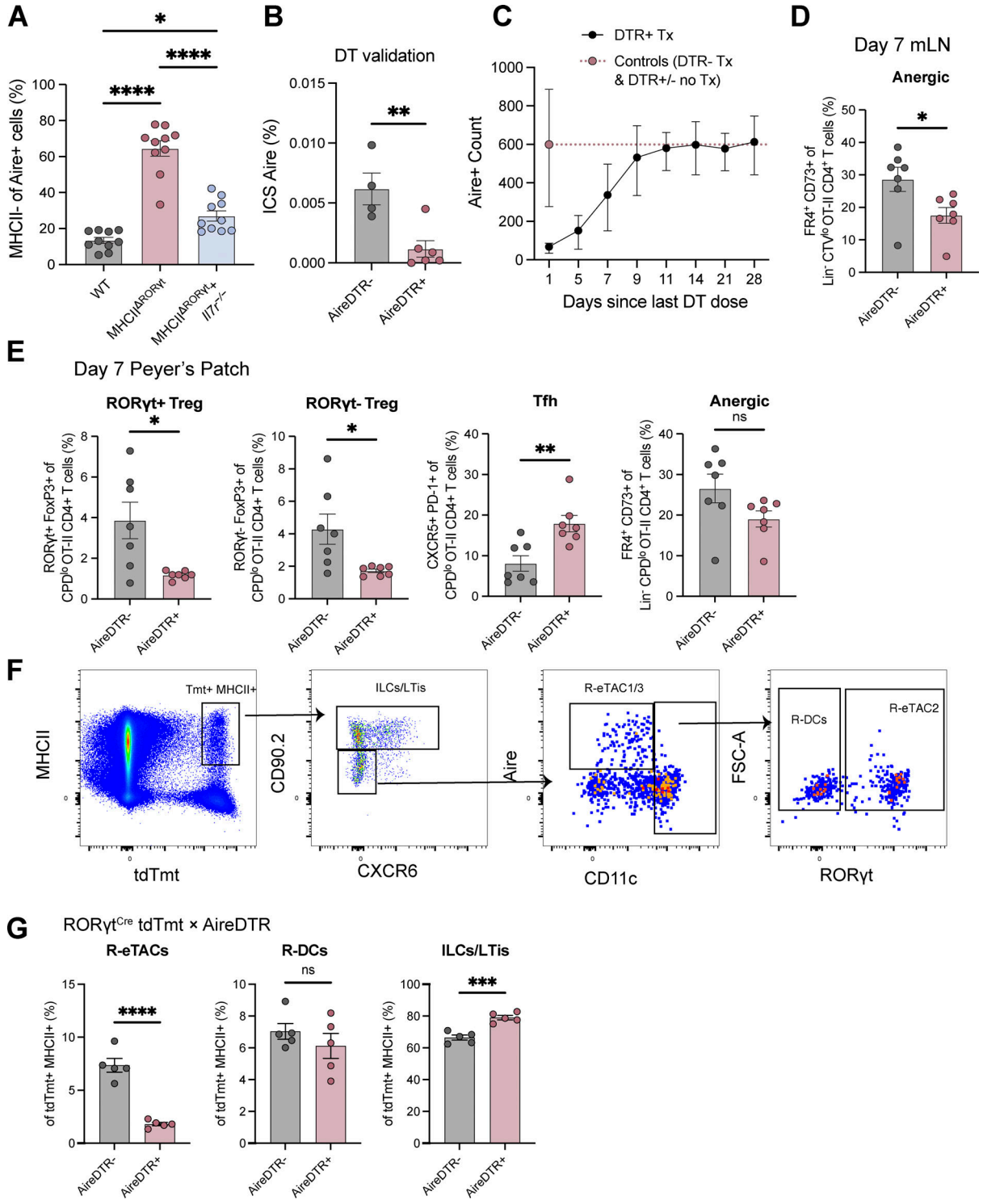

Figure S4. **R-eTACs enforce tolerance to dietary antigens.** Related to Fig. 4 A and Fig. 5. **(A)** Validation of MHC-II expression on Aire$^+$ cells in WT, MHCII$^{\Delta RORγt}$, and MHCII$^{\Delta RORγt}$ + *Il7r*$^{-/-}$ mixed BMC experiment from Fig. 4 A (n = 10 from each group). **(B)** Flow cytometry quantification of the AireDTR deletion of Aire$^+$ cells shown in Fig. 4 E. **(C)** Quantification of the repopulation kinetics of Aire$^+$ cells after DT treatment (n = 10 for controls [red], n = 2–4 for each experimental group time point [black]). Mice were treated with DT every other day for a total of five doses and collected at the time point indicated. **(D and E)** Experimental setup is the same as Fig. 5 B. **(D)** Quantification of anergic OT-IIs from the mLN after 7 days of oral OVA (n = 7 from each group). **(E)** Quantification of RORγt$^+$, RORγt$^-$ Treg, Tfh, and anergic OT-IIs 7 days after oral OVA in the PP (n = 7 from each group). **(F and G)** Flow validation of Aire$^+$ cell deletion in the spleen from the AireDTR$^+$×*RORγt*^{Cre}×Rosa26-LSL-tdTmt (AireDTR$^+$) BMC mice in Fig. 5 F. **(F)** Gating strategy for R-eTACs, R-DCs, and ILCs. **(G)** Quantification of RORγt-lineage APCs in the AireDTR×RORγt-lineage tracer mice (n = 5 from each group). Data in A, D, and E are pooled from two independent experiments. Data in B are representative of at least three independent experiments. Data in C are pooled from four independent experiments. Data in G is representative of two independent experiments. Error bars: mean ± SEM; statistics were calculated by one-way ANOVA with Tukey's multiple comparisons test (A) or unpaired two-sided t test (B, D, E, and G); *P < 0.05, **P < 0.005, ***P < 0.0005, ****P < 0.0001.

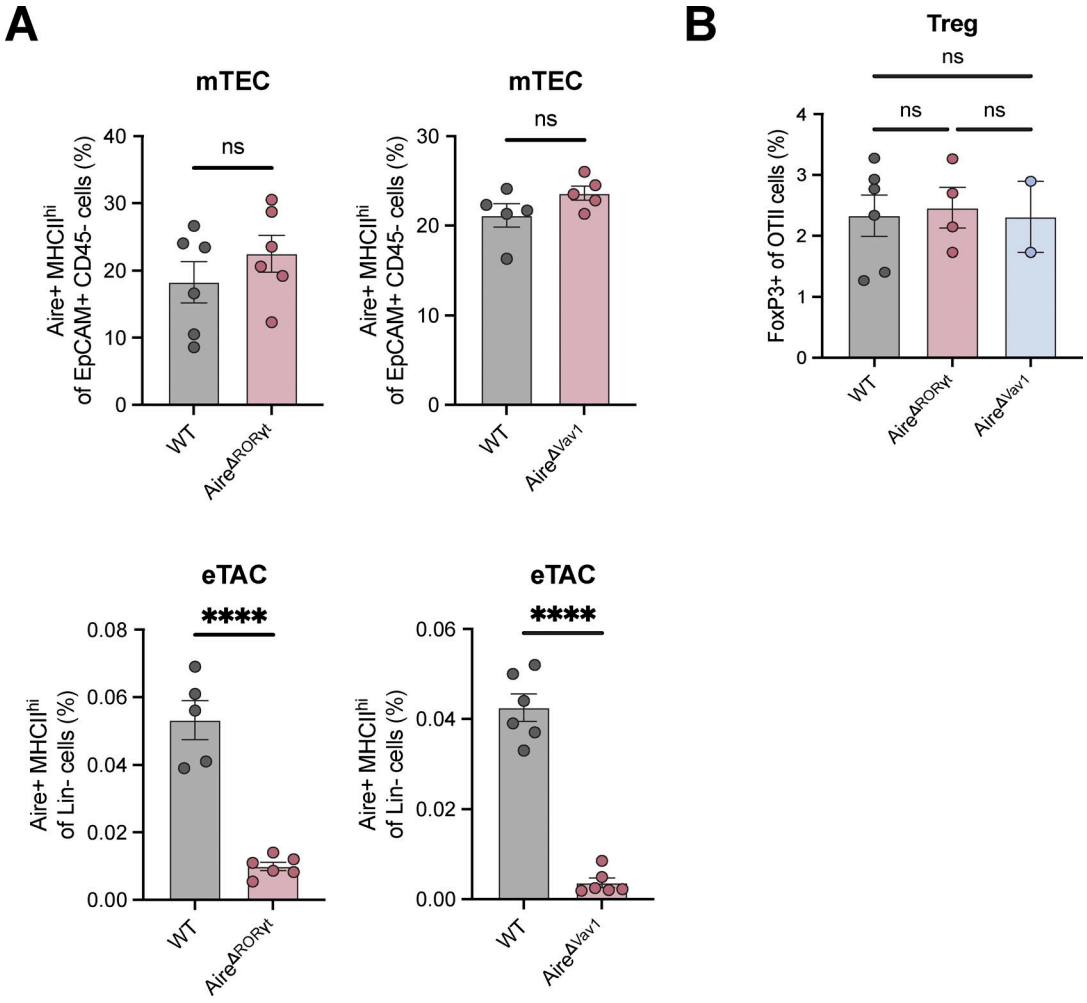

Figure S5. **Aire is dispensable in oral tolerance mediated by RORγt-lineage APCs. (A)** Quantification of Aire$^+$ MHCII$^+$ cells from the thymus (top) and LNs (bottom) in Aire$^{\Delta RORγt}$, Aire$^{\Delta Vav1}$, or WT mice (n = 6 from each group). **(B)** Oral tolerance experimental setup is the same as Fig. 1 A. Flow cytometry quantification of OT-II T cells from Aire$^{\Delta RORγt}$, Aire$^{\Delta Vav1}$, or WT mouse mLN after 2 days of OVA gavage (n = 6 for WT, n = 4 for Aire$^{\Delta RORγt}$, n = 2 for Aire$^{\Delta Vav1}$). Data are representative of three independent experiments. Error bars: mean ± SEM; statistics were calculated by an unpaired two-sided t test (A) and one-way ANOVA with Tukey's multiple comparisons test (B); ****P < 0.0001.

Provided online is Table S1. Table S1 lists differentially expressed genes from adult RORγt lineage–traced mice.